Aerosol activation in marine stratocumulus clouds: 2. Köhler and parcel theory closure studies

Jefferson R. Snider

Department of Atmospheric Science, University of Wyoming, Laramie, Wyoming, USA

Sarah Guibert and Jean-Louis Brenguier

Centre National de Recherche Météorologique (CNRM), Groupe de Météorologie Expérimentale et Instrumentale (GMEI/D), Météo-France, Toulouse, France

J.-P. Putaud

European Commission, Joint Research Centre, Institute for Environment and Sustainability, Ispra, Italy

Received 24 June 2002; revised 31 October 2002; accepted 31 January 2003; published 8 August 2003.

[1] Aerosol properties and vertical velocities relevant to cloud droplet concentrations in marine stratocumulus clouds are presented. Data were collected at a coastal surface site, and on an aircraft that flew north (upwind) of the surface site during the CLOUDYCOLUMN portion of the second Aerosol Characterization Experiment (ACE-2). In a closure study we compare observations, from five study days, and predictions based on Köhler and parcel theory. Measured and predicted cloud condensation nuclei (CCN) do agree after accounting for differences between the mobility equivalent (D_{me}) and sphere equivalent (D_{se}) diameters, but only when considering results from two study days unaffected by continental pollution. After applying the $D_{me} - D_{se}$ correction, cloud droplet concentration closure was also achieved, or nearly achieved, on three study days. Discrepancies between predicted and measured CCN, or between predicted and measured droplet concentration, were always in the direction of predicted values being larger than that measured. Although theoretical studies do specify scenarios where droplet concentration and CCN overestimation can occur, the observed disparities may also be due to multiple and poorly characterized experimental biases. *INDEX TERMS:* 0305 Atmospheric Composition and Structure: Aerosols and particles (0345, 4801); 0320 Atmospheric Composition and Structure: Cloud physics and chemistry; 1610 Global Change: Atmosphere (0315, 0325); *KEYWORDS:* aerosol indirect effect, CCN instrumentation

Citation: Snider, J. R., S. Guibert, J.-L. Brenguier, and J.-P. Putaud, Aerosol activation in marine stratocumulus clouds: 2. Köhler and parcel theory closure studies, *J. Geophys. Res.*, *108*(D15), 8629, doi:10.1029/2002JD002692, 2003.

1. Introduction

[2] Cloud condensation nuclei (CCN) instruments count particles that nucleate water condensation at water vapor pressures slightly in excess of saturation. The cumulative CCN concentration expressed as a function of applied supersaturation, commonly known as the CCN activation spectrum, is the basis for describing the early stages of droplet growth in clouds. Studies of both cumulus and stratiform clouds have validated the parcel theory that links CCN activation spectra, vertical velocity, and cloud microphysical properties [*Twomey and Warner*, 1967; *Fitzgerald and Spyers-Duran*, 1973; *Yum et al.*, 1998; *Snider and Brenguier*, 2000]. In contrast, attempts made to link aerosol size spectra and cloud microphysical properties have not been as successful [*Hallberg et al.*, 1997, 1998]. Lack of closure in the latter experiments puts into question climate model predictions that utilize aerosol size spectra for diagnosing cloud droplet number concentration [*Ghan et al.*, 1993; *Abdul-Razzak and Ghan*, 2000] and also points to inadequate understanding of a fundamental aspect of warm cloud microphysics. This deficiency may either reflect biases in the measurements or may arise because of invalid assumptions or approximations in the equations used to model atmospheric condensation nucleation.

[3] Here we examine airborne- and surface-based measurements made in June and July of 1997 during the CLOUDYCOLUMN portion of the second Aerosol Characterization Experiment (ACE-2). Two aspects of the aerosol activation problem are addressed. First, we evaluate aerosol size spectra, measured at a coastal surface site, and assess their consistency with airborne CCN activation spectra measurements. The former were intercompared with airborne measurements in the first paper of this special section [*Guibert et al.*, 2003], hereinafter referred to as part 1. Second, we compare observations and predictions of cloud droplet number concentration (CDNC).

[4] Figure 1 illustrates the methodology used in this paper. Comparisons are made between cumulative CCN concentration (N_o, Figure 1a) and integrations of an aerosol differential size spectrum from large size down to a spec-

0148-0227/03/2002JD002692$09.00

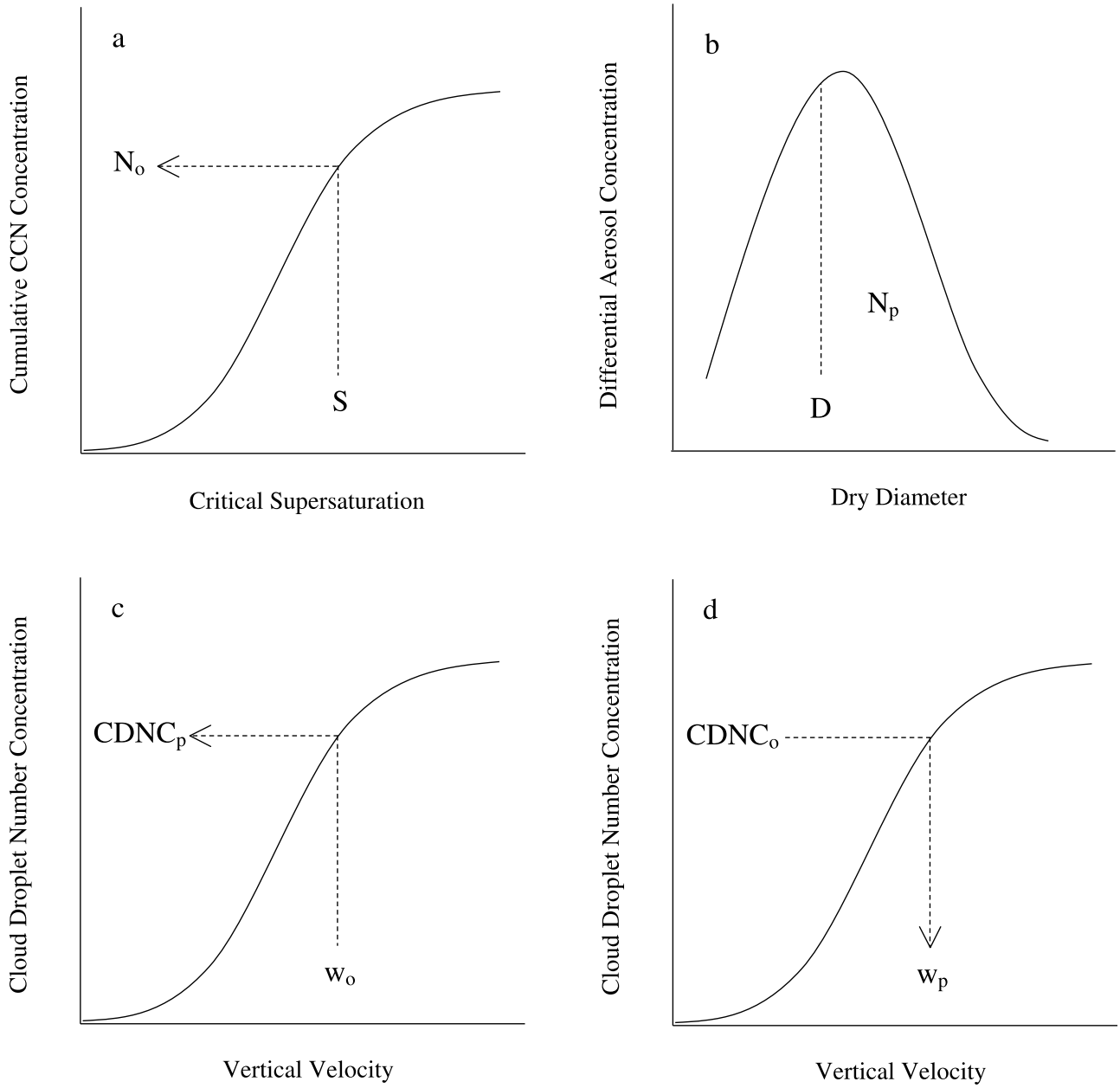

Figure 1. Graphical representations of the methodology used to compare cumulative CCN concentration and size-integrated aerosol concentration (Figures 1a and 1b), to predict CDNC for comparison with measurements (Figure 1c), and to predict vertical velocity for comparison to measurements (Figure 1d). See text for details.

ified dry size D (N_p, Figure 1b). This comparison is based on measurements which indicate that the submicron aerosol is internally mixed. The link between critical supersaturation and dry particle diameter (Figures 1a and 1b) is provided by Köhler theory. Also compared are observations of CDNC, conditionally sampled from cloud regions unaffected by loss due to either droplet evaporation or drizzle scavenging, and CDNC predictions based on either measured aerosol size spectra or CCN activation spectra. The comparison of observed and predicted CDNC is statistical because a distribution of vertical velocities is observed and thus a range of CDNC is expected even if aerosol or CCN spectra are constant. The predicted distribution of CDNC is calculated using parcel model predictions of the relationship between CDNC and vertical velocity (Figure 1c) and vertical velocity probability distribution functions. The final comparison, shown in Figure 1d, is conducted between measured vertical velocities and those that force agreement between observed and predicted CDNC.

[5] Our approach is unique since we evaluate a data set that includes measurements of the six relevant parameters: CDNC, vertical velocity, CCN activation spectra, aerosol size spectra, aerosol chemical composition, and aerosol growth factors. Some of the work conducted previously

utilized model estimates of vertical velocity and did not have measurements of CCN to compare to predicted CCN activation spectra [*Hallberg et al.*, 1997, 1998]. In our presentation we refer to the suite of measurements used to predict CCN activation spectra (i.e., aerosol size spectra and aerosol chemical composition) as aerosol physicochemical properties. Other investigators have predicted CCN activation spectra from aerosol physicochemical property data and compared those to measured CCN [*Fitzgerald*, 1973; *Bigg*, 1986; *Quinn et al.*, 1993; *Covert et al.*, 1998; *Chuang et al.*, 2000; *Wood et al.*, 2000; *Cantrell et al.*, 2001; *Zhou et al.*, 2001]. However, none of those investigators had at their disposal a data set that allowed both comparisons, i.e., predicted and observed CCN, and predicted and observed CDNC.

[6] This work is divided into five sections. First (section 2), we present the measurements used in the analysis. That section concludes with a discussion of laboratory studies conducted using the CCN instrument which was used in the field during ACE-2. The laboratory studies characterize the response of the CCN instrument to particles of known composition and mobility-selected size. That result is used in section 3 to estimate errors in the comparison predicted and observed CCN activation spectra. We refer to this exercise, illustrated in Figures 1a–1b, as the "static closure." Next (also section 3), we present measured CDNC values and compare those to predictions based on a parcel model, initialized with two dry size spectra (one derived from CCN activation spectra measurements and the other measured directly). We refer to this second exercise, illustrated in Figure 1c, as the "kinetic closure." The results of both closure studies are discussed and our overall conclusions are presented in sections 4 and 5, respectively. In section 3 we also provide short descriptions of the Köhler theory and parcel models used in the static and kinetic closure studies. Complete descriptions of the models are provided in Appendix A.

2. Measurements

2.1. Surface Measurements

[7] Measurements made at the ACE-2 surface site [*Putaud et al.*, 2000; *Swietlicki et al.*, 2000], located on the north coast of the Canary island of Tenerife, are used in this study. Discussed here are the measurements of aerosol size spectra, submicron aerosol chemical composition and submicron aerosol growth factor made at the surface site.

2.1.1. Aerosol Size Spectra

[8] At the surface site, aerosol was drawn through an inlet that transmitted particles larger than 15 μm. Aerosol within the inlet were heated by ~5°C and sampled by two particle size spectrometers. The measurement systems were a Vienna type differential mobility analyzer (DMA), operated in stepping mode, for particles in the 0.006 to 0.5 μm mobility equivalent size range, and a TSI 33B Aerosol Particle Sizer (APS) for particles in the 0.50 to 29 μm aerodynamic size range. Intercomparisons reported by *Putaud et al.* [2000] and by *Van Dingenen et al.* [1999] show that the integrated concentrations reported by the APS and the DMA are made with a relative precision of ±5% and ±10%, respectively.

[9] Size spectra were screened to eliminate time intervals not associated with onshore flow and averaged over the flight intervals of the research aircraft (i.e., the Météo-France Merlin, hereinafter referred to as the M-IV). The averaging intervals were 1150 to 1450 UT (26 June), 1240 to 1550 UT (9 July), 1200 to 1550 UT (17 July), and 1300 to 1700 UT (18 July) for four of the five study days analyzed in this paper (criteria used to select these study days are presented in section 2.2). On 25 June, surface site data are only available for the first 50 min of the M-IV flight interval (1100 to 1150 UT).

[10] Implicit in our analysis of the size spectra are three assumptions. First, we assume that the particles were sized dry. This is consistent with the fact that air inside the inlet was heated by ~5°C relative to the ambient state, by the fact that the relative humidity (RH) of the DMA sheath air was 20 ± 10% [*Putaud et al.*, 2000], and by the fact that the temperature of aerosol entering the APS was increased by 10°C relative to that inside the inlet. Second, we assume that the mobility equivalent diameter, classified by the DMA, is equal to the sphere equivalent diameter. The latter is defined as the diameter that would result if the dried particle were compacted to form a sphere of density prescribed by our aerosol model (section 3.1.1). Model-predicted values of aerosol density at relevant dry sizes ($D <$ 0.50 μm) range between 1730 and 1750 kg/m^3 depending on soluble mass fraction (section 2.1.3) and model assumptions justified in section 3.1.1. Third, the aerodynamic diameters measured by the APS (0.50 to 29 μm) were converted to sphere equivalent diameters (0.38 to 22 μm) on the assumption that the actual particles were spheres of density 1700 kg/m^3. Throughout this paper DMA and APS data will be plotted as functions of the assumed sphere equivalent diameters; however, axes labels will only designate "Dry Diameter."

[11] Averaged size spectra from 26 June and 9 July, the two study days showcased in part 1, are shown in Figure 2. DMA averages are symbolized by triangles and APS averages by squares. Note that the spectra are expressed as count mixing ratios (number per milligram of air) per unit decimal logarithmic size. The short vertical lines overlain on the spectral densities indicate sample variability expressed as plus or minus one standard deviation. At sizes larger than 0.03 μm spectra densities do not vary substantially during the sampling intervals, indicating that the surface site spectra are stable at dry sizes relevant to the problem of cloud droplet nucleation in marine stratocumulus clouds (i.e., ~0.05 μm and larger).

[12] Prominent modes are evident at 0.05, 0.16 and 0.50 μm; we refer to these as the Aitken, accumulation, and large modes, respectively. The positions of the largest two modes are consistent with the marine aerosol climatology of *Gras* [1995]; however, the Aitken mode size is about a factor of 2 larger than that reported by *Gras* [1995].

[13] In the 0.38 to 0.50 μm size range the APS underestimates spectral densities reported by the DMA. This disparity is attributed to the low APS counting efficiencies at the lower end of the APS range (E. Sweitlicki, private communication), and accordingly, we have relied on APS measurements at sizes larger than 0.78 μm, and on DMA measurements in the 0.2 to 0.5 μm size range, to derive a bimode lognormal fitting function. The fit, indicated by the solid line in Figure 2, is used in our model to describe the aerosol spectrum at sizes larger than 0.50 μm. The aerosol

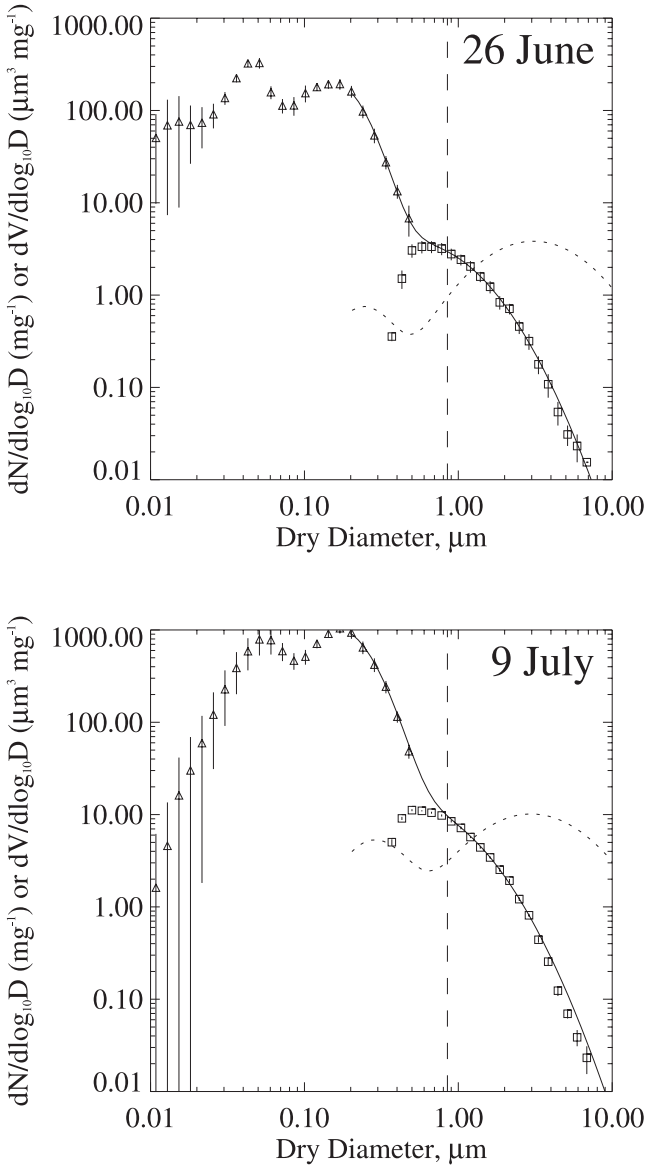

Figure 2. Aerosol spectra measured on 26 June (top) and 9 July (bottom). Triangles and squares represent averages from the DMA and APS instruments, respectively. For clarity, only every other measured spectral density value is plotted. Short vertical lines indicate the averages plus or minus one standard deviation. The solid curve is a fit of combined DMA and APS measurements, and the dotted curve is the corresponding aerosol volume spectrum. The dashed vertical line is the dry size cut of the virtual impactor used for filter sampling (0.85 μm [*Putaud et al.*, 2000]).

volume spectra calculated using the fit (dotted curve) peak at approximately 0.2 and 3 μm. Aerosol mass loadings derived by integrating the volume spectra at sizes larger than 1 μm, and based on the assumption that the particle density is 1700 kg/m^3, are consistent with ACE-2 measurements reported by *Quinn et al.* [2000]. They show that large mode mass loadings range between 2 and 18 μg/m^3 with an average and standard deviation of 9 ± 4 μg/m^3. Results from the five study days considered here range between 4 and 19 μg/m^3 with an average and standard deviation of 9 ± 6 μg/m^3.

2.1.2. Aerosol Chemical Composition

[14] Filter sampling of the aerosol was conducted downstream of a virtual impactor [*Putaud et al.*, 2000]. Ambient (wet) particles of aerodynamic size smaller than 1.26 μm were transmitted to the filter substrates. Assuming sphericity, a dry particle density (1700 kg/m^3), averaged ambient RH (72%) and a growth factor (1.38 at RH = 72%), the dry particle cut diameter of the virtual impactor is 0.85 μm [*Putaud et al.*, 2000]. A vertical dashed line in Figure 2 indicates the 0.85μm cut diameter. Following Putaud et al., we refer to the aerosol fraction collected at the surface site as the submicron aerosol.

[15] The submicron aerosol chemical composition data correspond to samples collected over 11-hour sample intervals, started at 0800 UT. The M-IV flew north of the surface site starting as early as 1100 UT, and ending as late as 1700 UT (section 2.1.1). The submicron aerosol chemistry data set consists of measurements of water-soluble inorganic and organic ions, inorganic and organic carbonaceous species, and elements linked to terrestrial dust sources. *Putaud et al.* [2000] compared chemically derived, size-spectrum-derived, and gravimetric aerosol mass measurements. Those comparisons do not reveal any bias and indicate that the relative uncertainty is ±40% for the chemically derived/gravimetric mass comparison and ±50% for the chemically-derived/size-spectrum-derived mass comparison. Implicit in the latter is the assumption that the dry particle density is 1700 kg/m^3.

2.1.3. Aerosol Soluble Fraction

[16] As was mentioned in the introduction, Köhler theory is used to transform between dry particle diameter and critical supersaturation. A parameter in the theory is the fraction of the aerosol mass that is water-soluble. For what we refer to as the "nominal" solubility scenario, the water-soluble mass fraction (ε) was taken to be the sum of submicron mass speciated as water-soluble ions (i.e., organic acid anions, NaCl, non-sea salt sulfate, ammonium and nitrate) divided by the total aerosol mass. ACE-2 nominal soluble fraction values are reported in *Snider and Brenguier* [2000]. Here we also consider a "lower limit" solubility defined as the nominal soluble fraction reduced by 40%, a result consistent with the error analysis of *Putaud et al.* [2000]. Further, we define the "upper limit" soluble fraction by classifying 50% of the organic carbonaceous mass as water-soluble. Support for this assumed upper limit comes from the work of *Novakov et al.* [2000]. Nominal soluble fractions and their upper and lower limits are presented in Table 1. Also shown are measurements of total mass loading (i.e., the sum of the individual chemical mass measurements reported by *Putaud et al.* [2000], the non-sea salt sulfate and NaCl mass loadings, and the ammonium-to-sulfate mole. Like soluble fraction, these additional chemical properties were derived using the aerosol composition data reported by *Putaud et al.* [2000]. Results presented in Table 1 indicate the following: (1) nominal soluble fraction values range between 0.48 (26 June) and 0.75 (25 June and 9 July), (2) ammonium, sulfate and total mass values are approximately an order of magnitude larger on the three polluted days (9, 17 and 18 July (part 1)) compared to that observed on the two unpolluted days (25 and 26 June

Table 1. Submicron Aerosol Composition[a]

Date	Nominal ε	Upper ε	Lower ε	Total Mass, $\mu g/m^3$	nss-SO_4 Mass, $\mu g/m^3$	NaCl Mass, $\mu g/m^3$	NH_4-to-SO_4 Mole Ratio
25 June	0.75	0.87	0.45	0.7	0.2	0.2	1.9
26 June	0.48	0.61	0.29	1.2	0.2	0.2	2.0
9 July	0.75	0.85	0.45	5.8	2.8	0.6	1.7
17 July	0.63	0.77	0.38	3.4	1.6	0.1	1.7
18 July	0.73	0.82	0.44	5.9	3.1	0.1	1.7

[a]Concentrations are reported at standard temperature (273 K) and pressure (1013 hPa).

(part 1)), (3) combined, ammonium and sulfate constitute between 29 and 62% of the mass, (4) NH_4-to-SO_4 mole ratios are nearly consistent with that expected for ammonium sulfate ($(NH_4)_2SO_4$), and (5) one of the polluted cases (9 July) has enhanced levels of NaCl (i.e., 0.6 $\mu g/m^3$ versus 0.1 to 0.2 $\mu g/m^3$).

2.1.4. Growth Factor

[17] *Swietlicki et al.* [2000] report DMA measurements of dry particle size and wet particle size at RH = 90%. The parameter they report is the ratio of the wet particle size divided by the dry particle size. This is called the growth factor and is reported for dry sizes equal to 0.04, 0.05, 0.07, 0.11, 0.17, 0.26 and 0.44 μm. Measurements at 0.44 μm are not available for any of the time intervals we analyze in this work. Relative uncertainty in the growth factor measurement is ±5% [*Swietlicki et al.*, 2000].

2.2. Aircraft Measurements

[18] M-IV cloud microphysical measurements obtained during ACE-2 were analyzed by *Pawlowska and Brenguier* [2000]. Part 1 shows that one of the eight flights analyzed by *Pawlowska and Brenguier* [2000] was conducted ~600 km north of the surface site, and that two of the eight flights were associated with spatially nonuniform boundary layer aerosols. Four of the remaining five flights were conducted within ~100 km of the surface site (25 and 26 June, 9 and 17 July) and a fifth flight (18 July) was con-ducted 140 km farther north. Here, we analyze data from those five flights. Flight tracks are plotted in Figure 2 of part 1.

[19] Part 1 also presents comparisons of surface- and aircraft-based condensation nuclei (CN, D > 0.01 μm) and accumulation mode (0.1 < D < 0.5 μm) aerosol concentrations. With the exception of the three cases excluded in the previous paragraph, the aerosol concentration comparisons revealed no bias and showed that airborne- and surface-based averages agree within ±20%. Those results corroborate the assumption, implicit in this analysis, that surface-based aerosol physicochemical measurements are representative of the marine boundary layer north of the Canary Island of Tenerife. Complicating that assessment are results which show that accumulation mode aerosol measurements made by the M-IV, via a reverse-facing inlet, are negatively biased due to inefficient aerosol transmission into a Particle Measurement Systems (PMS) passive cavity aerosol spectrometer probe (PCASP) operated within the aircraft fuselage. As is discussed in part 1, this bias was characterized when switching the PCASP from the reverse-facing inlet to a forward-facing quasi-isokinetic inlet during test flights conducted on both 21 and 22 July 1997. It should be pointed out that the CCN instrument operated on the M-IV (section 2.3) sampled from the forward-facing quasi-isokinetic inlet and that particle transmission efficiency for that M-IV inlet is assumed to be unity. Measurements from the M-IV PCASP are not used in this analysis.

[20] The M-IV CCN and CN data used in this analysis are restricted to samples obtained from below-cloud regions containing no cloud droplets or drizzle drops (CDNC < 2 cm^{-3} and drizzle concentration <2 cm^{-3}), as both artificially increase the measured CN concentration [*Snider and Brenguier*, 2000].

2.2.1. Cloud Droplet Number Concentration

[21] CDNC measurements were made on the M-IV with the Fast-FSSP, an improved version of the standard FSSP-100 airborne droplet spectrometer [*Brenguier et al.*, 1998]. The CDNC was derived as $CDNC = C/(z \cdot u \cdot \Delta t)$, where C is the number of droplets counted in a sample, z is the sampling section, u is airspeed, and Δt is the sample duration. The quantity $C/\Delta t$ is referred to as the droplet rate. Errors in the estimation of the droplet rate may arise from particles that are undetected because they are smaller than the minimum detectable diameter (2.6 μm). This potential bias was avoided by *Pawlowska and Brenguier* [2000], who restricted their analysis of M-IV measurements to droplet size spectra observed within the center of the cloud layer. Further explanation of the CDNC sampling procedure employed by Pawlowska and Brenguier is provided in section 3.2.2.

[22] Droplet coincidence in the Fast-FSSP sampling section is also a source of droplet rate underestimation. Indeed, the results obtained by *Martinsson et al.* [2000] do reveal a large (factor of 2) underestimation of CDNC at values in excess of 1000 cm^{-3}. Since the CDNC values observed by the Fast-FSSP flown on the M-IV are smaller than 1000 cm^{-3}, and because there is no need for a dead-time correction of the Fast-FSSP data [*Brenguier et al.*, 1998], in contrast to the standard FSSP-100 used by Martinsson et al., it is unlikely that the phenomenon they document is of relevance to the Fast-FSSP CDNC measurements. CDNC uncertainty also originates from uncertainty in laboratory determination of the sampling section and from error in the airspeed. FSSP intercomparisons conducted by *Burnet and Brenguier* [2002] indicate that combined these CDNC uncertainties can be as large as ±30%. Note that if uncertainty in the measurement of CDNC dominates, an upper limit value for the predicted-to-observed CDNC ratio is 1.0/0.7 or 143%.

2.2.2. Vertical Velocity

[23] Vertical velocity (w) was obtained from a differential-pressure sensor mounted on the nose radome of the M-IV. We refer to this sensor as the gust probe. Values of

w were selected from level-flight traverses of the cloud layer and were sampled at 10 Hz. When expressed as a standard deviation, the widths of the flight-averaged probability distribution functions pdf(*w*) ranged between 0.4 m/s (17 July) and 0.6 m/s (18 July). These standard deviations are ~0.1 m/s larger than the standard deviations reported by *Snider and Brenguier* [2000] who used 1 Hz, as opposed to 10 Hz, M-IV gust-probe data. The small increase occurred because *Snider and Brenguier* [2000] considered relatively short flight sections while here the vertical velocity statistics are based on all straight and level in-cloud segments. Average and median vertical velocities differ by less than 0.03 m/s, both for the *Snider and Brenguier* [2000] probability distribution functions and for those reported here. The averaged values of *w* do indicate a positive bias. That bias is smallest for the flight conducted on 17 July (0.0 m/s) and largest for the flight conducted on 26 June (0.3 m/s). *Brown* [1993] conducted an error analysis of vertical velocity measurements made by a gust probe similar to that used on the M-IV. Random and systematic errors are 0.1 m/s and 0.3 m/s, respectively. On the assumption that bias associated with individual values of *w* are a constant for any flight we removed the pdf(*w*) average from each sample and used the unbiased measurements to reconstruct an unbiased pdf(*w*). The portion of the unbiased pdf(*w*) larger than 0.0 m/s is referred to as the "truncated vertical velocity probability distribution function" and this is used for predicting CDNC.

2.3. Cloud Condensation Nuclei (CCN)

[24] Two CCN measurement uncertainties are evaluated in this section. The first or "type-1" error originates from the calibration used to infer activated droplet concentrations, and therefore CCN, from measurements of scattered light intensity made with the University of Wyoming (UWyo) CCN instrument (serial number CCNC-100A-104). As is described by *Snider and Brenguier* [2000], the CCN calibration is based on video measurements of droplets that activate in a short (1 cm) section of the illuminating laser beam. The beam is focused through the middle of the CCN chamber. The derived calibration slope, defined by linear fits of the video droplet count plotted versus scattered light intensity, might be negatively biased because of improper alignment of the video camera [*Delene and Deshler*, 2000]. Figure 3 shows calibration slopes plotted as a function of applied supersaturation and the fit used to derive concentration data from field measurements of scattered light intensity. The calibration slopes used to construct the fit correspond to laboratory calibrations conducted during September of 1997, 1 month after the end of the field experiment (June–July 1997). At the lowest supersaturation (0.2%), the September 1997 calibration slope is smaller than two subsequent results. At 0.4% one of the calibration slopes plots above the September 1997 result. Based on the January 1998 and September 1998 calibrations, and their comparison to the September 1997 calibrations, the type-1 error, expressed as a systematic bias, was estimated as

$$\frac{[CCN_{\text{actual}}]}{[CCN_{\text{biased}}]} = 1.3 \qquad S < 0.6\% \tag{1}$$

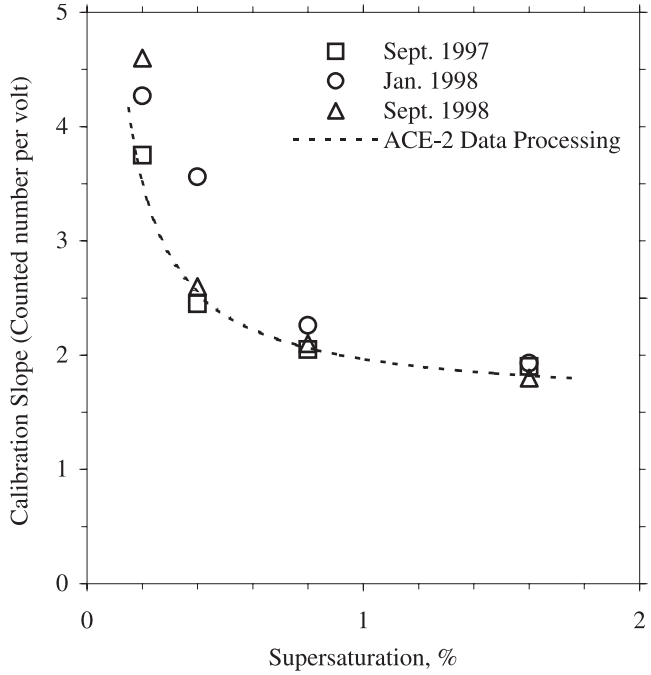

Figure 3. Calibration data for supersaturations 0.2 to 1.6% obtained using the video technique of *Delene and Deshler* [2000]. The calibration slope is obtained by plotting peak photodetector voltage versus the droplet count in the video sample volume. Calibrations used to process the ACE-2 results, conducted in September 1997, were fitted to a function having the form: Calibration slope = $A + B/S$.

and

$$\frac{[CCN_{\text{actual}}]}{[CCN_{\text{biased}}]} = 1.0 \qquad S > 0.6\% \tag{2}$$

Here $[CCN_{\text{actual}}]$ is the concentration, obtained after correcting for the type-1 error, $[CCN_{\text{biased}}]$ is the concentration obtained using the ACE-2 calibration result (dashed line, Figure 3), and S is the applied supersaturation. Although we treat the type-1 error as a bias, the correction implied by (1) and (2) might also represent the upper limit of a poorly characterized random error.

[25] The type-2 error results from uncertainties associated with the applied supersaturation. Here it is important to recognize that direct measurement of the applied supersaturation is not possible, rather it is inferred using measurements of the temperature difference imposed across the plates that define the top and bottom of the CCN chamber [*Katz and Mirabel*, 1975]. We routinely compare the inferred supersaturation to predictions based on Köhler theory. This is done by testing the CCN instrument with quasi-monodisperse aerosols prepared in a four step process: (1) aqueous $(NH_4)_2SO_4$ or NaCl solution nebulization (TSI 3075 Constant Output Atomizer), (2) polydisperse aerosol drying (TSI 3062 Diffusion Dryer), (3) charge neutralization (TSI 3012 Aerosol Neutralizer) and (4) mobility selection (TSI 3071 Electrostatic Classifier). The electrostatic classifier was operated using a sheath to sample flow rate ratio of 5 to 1. Mode sizes between 0.02 and

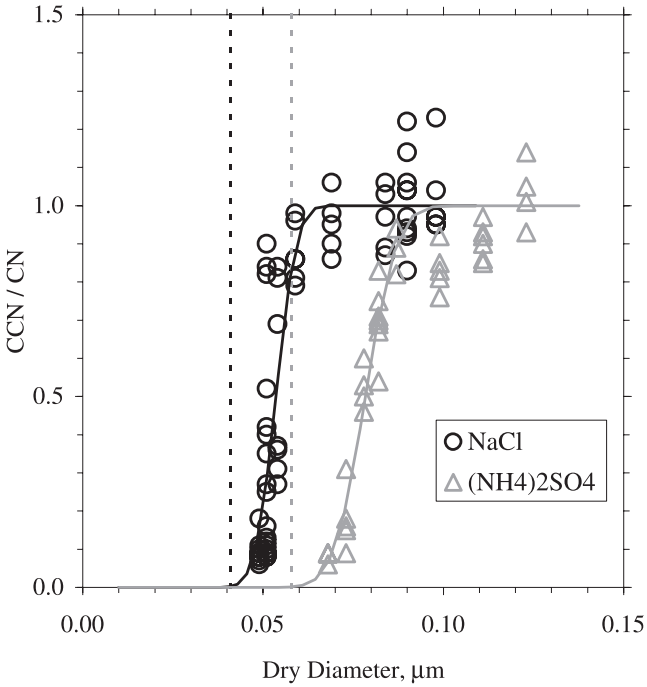

Figure 4. Comparison of observed and predicted dry sizes that activate in the UWyo CCN instrument. Data were collected at an applied supersaturation equal to 0.4%. The dashed vertical lines are predictions based on $S = 0.4\%$ and Köhler theory. The fitting function is a normalized Gaussian.

0.14 μm were selected and the base width of the selected modes ranged between 0.004 to 0.034 μm in accordance with both electrostatic classifier theory [*Knutson and Whitby*, 1975] and size spectra measurements made with a Scanning Mobility Particle Sizer (TSI 3936L10). Concentrations of the quasi-monodisperse particles were measured with a TSI 3010 condensation particle counter and their concentration was maintained within ±30% of 300 cm^{-3}. Since the test particles were sized at RH = 10%, and their efflorescence RH is larger [*Tang*, 1996; *Tang and Munkelwitz*, 1994], they were assumed to be completely dried. The chamber supersaturation that we infer from the CCN response to particles selected based on their electrical mobility is called the theoretical chamber supersaturation.

[26] Results are shown in Figure 4 where the CCN-to-CN concentration ratio is plotted versus mobility-selected dry size for measurements made at an applied supersaturation equal to 0.4%. Solid lines are the fitted activation efficiency curves, from which a 50% activation size is inferred. The dashed vertical lines indicate theoretical predictions of the activation size based on a Köhler theory model evaluated at $S = 0.4\%$. Our formulation of Köhler theory is described in Appendix A. These results show that the 50% activation size is substantially larger than that predicted using the Köhler model. Further, results presented in Table 2 show that there is a consistent bias between the applied (based on measured differential temperature and *Katz and Mirabel* [1975]) and the theoretical (based the 50% activation size and Köhler theory) supersaturations. This is apparent both for prepared ammonium sulfate and sodium chloride aerosols. Based on the results shown in Table 2 the type-2 error was estimated as

$$\frac{S_{\text{theory}}}{S_{\text{applied}}} = 0.52 \qquad 0.2 < S < 0.3 \tag{3}$$

and

$$\frac{S_{\text{theory}}}{S_{\text{applied}}} = 0.65 \qquad 0.3 < S < 1.6 \tag{4}$$

[27] The type-2 error could be due to errors in the temperature or vapor pressure difference controlled between the wetted blotter paper at the top and bottom plates of the CCN chamber. The temperature difference measurement is computed from an analog signal produced by a matched pair of thermocouples. These are imbedded in the top and bottom plates which are constructed from aluminum. Measurements made with a second set of thermocouples, both attached to the inner plate surfaces, and compared to the temperature difference derived from the imbedded thermocouples, differ by less than 0.3°C. At an applied supersaturation of 0.4% this means that actual supersaturation could be as small as 0.35% (+12% relative error). Clearly, this is insufficient for explaining the supersaturation disparity reported in Table 2.

[28] Remaining is the possibility that the water vapor pressure is overestimated. Here it is important to note that the procedure we use to infer the applied supersaturation [*Katz and Mirabel*, 1975] assumes that the water vapor pressure at the blotter paper surfaces corresponds to that expected for a flat surface of pure water [*List*, 1984]. Overestimation could occur if the blotting paper, or solute dissolved in the water used to wet the blotting paper, alters the water activity. For example, a 0.1% reduction in vapor pressure occurring at the paper surfaces reduces the supersaturation in the center of the chamber, where it is a

Table 2. Summary of the Type-2 Error for Ammonium Sulfate and Sodium Chloride[a]

S_{applied}, %	Theoretical Dry Diameter at S_{applied}, μm	50% Activation Dry Diameter, μm	S_{theory},%	$S_{\text{theory}}/S_{\text{applied}}$
		$(NH_4)_2SO_4$		
0.2	0.092	0.141	0.11	0.53
0.4	0.058	0.078	0.26	0.64
0.8	0.037	0.048	0.53	0.66
1.6	0.023	0.032	0.99	0.62
		NaCl		
0.2	0.065	0.102	0.10	0.50
0.4	0.041	0.055	0.26	0.64
0.8	0.026	0.037	0.47	0.58
1.6	0.016	NA	NA	NA

[a] S_{applied} is based on a steady state model of the CCN chamber [*Katz and Mirabel*, 1975] and measurements of the temperature difference controlled between the top and bottom plates. The theoretical dry diameter is the dry size, predicted by Köhler theory, corresponding to a critical supersaturation equal to S_{applied}. The 50% activation dry diameter is defined as the size that predicts, via the fits shown in Figure 4, CCN/CN = 0.5. S_{theory} is the critical supersaturation, predicted by Köhler theory, evaluated at the 50% activation dry diameter. NA = not available.

Table 3. Laboratory Determinations of the Sphere Equivalent (D_{se}) and Mobility Equivalent (D_{me}) Diameter[a]

Aerosol	Measurement	D_{se}/D_{me}	Reference
0.05 μm NaCl produced by atomization	aerodynamic and mobility size	0.93[b]	*Kelly and McMurry* [1992]
Monodisperse 0.05 to 0.2 μm PSL produced by atomizing PSL/water suspensions	gravimetric- and SMPS-derived aerosol mass concentration	0.85 to 0.87[c]	*Sioutas et al.* [1999]
Polydisperse K_2SO_4 produced by atomization	gravimetric- and SMPS-derived aerosol mass concentration	0.80 to 0.94[c]	*Sioutas et al.* [1999]
0.05 μm NaCl produced by atomization	growth factor	0.96[b]	*Hämeri et al.* [2001]

[a]SMPS is the Scanning Mobility Particle Sizer (TSI Inc.).
[b]D_{se}/D_{me} derived as the cube-root of the ratio of the inferred and bulk densities.
[c]D_{se}/D_{me} derived as the cube-root of the ratio of the gravimetrically derived and SMPS-derived aerosol mass concentration ratio.

maximum, by about 30%. Evidence against this come from the fact that the hypothesized error varies strongly with applied supersaturation when in fact the error documented in Table 2 is relatively constant for a broad range of applied supersaturation (S = 0.2 to 1.6%).

[29] The type-2 error may also result from the particle size ambiguity documented in Table 3. To demonstrate the effect we consider two measures of particle size, the sphere equivalent and the mobility equivalent diameters (i.e., D_{se} and D_{me}, respectively). The former is defined in section 2.1.1, and the latter is defined in terms of the drag force exerted on particles within a DMA. If the ratio D_{se}/D_{me} is assumed equal to 0.9, then the critical supersaturation ratio ($S_c(D_{me})/S_c(D_{se})$) is 0.85. For a D_{se}/D_{me} of 0.8, the lowest value given in Table 3, $S_c(D_{me})/S_c(D_{se})$is 0.71. These calculations presume that D_{se} is 0.07 μm, that the particles are composed of ammonium sulfate, and are based on our Köhler model. The calculations, and laboratory data presented in Table 3, suggest that particles selected by a DMA can carry significantly less mass than is expected when assuming that D_{me} is that same as D_{se}. Reasons for this disparity include both asphericity and porosity, as is discussed by *Hinds* [1999], and also the unexpected presence of water as a component of dried laboratory aerosols [*Weiss and Ewing*, 1999]. If the laboratory determinations of D_{se}/D_{me} (Table 3) can be extended to the ambient aerosols during ACE-2, then a substantial part of the type-2 error may be attributed to the incorrect assumption (section 2.1.1) that D_{se} is equal to D_{me}.

[30] Although we cannot rule out the possibility that the type-2 error is the result of overestimation of the applied supersaturation, the result presented in Table 3 suggests that a portion of that disparity may be attributable to overestimation of the salt mass associated with particles selected based on their electrical mobility. Because both that effect and the hypothesized effect of reduced vapor pressure at the blotter paper surfaces are substantial, and neither is adequately constrained, an acceptable closure result is not expected. Our results confirm that suspicion, at least for two of five study days we analyze. To help reconcile the lack of closure we evaluate the degree to which the discrepancy can be diminished by applying the CCN data corrections (i.e., equations (1), (2), (3), and (4)) to the field CCN measurements, and we also assess sensitivity to the assumption that D_{me} is equal to D_{se}. For the latter we use D_{se}/D_{me} = 0.8 and apply that correction only to size spectra measurements made with the surface site DMA (D < 0.5 μm).

3. Results

3.1. Static Closure

[31] Two aspects of the static closure problem are examined in this section. First (section 3.1.1), we consider growth factor measurements made at the surface site [*Swietlicki et al.*, 2000]. Those results are analyzed with the submicron aerosol chemistry data [*Putaud et al.*, 2000] and used to constrain Köhler model predictions of aerosol growth at RH less than 100%. Implicit in the model, and in the parcel model which initializes using the Köhler model, is the assumption that the submicron aerosol is internally mixed with regard to its hygroscopic properties. That assumption implies the existence of only one hygroscopic growth mode, and if supported by observations lends support to the additional assumption that the aerosol is also internally mixed chemically. The presumption of a single hygroscopic mode is consistent with the overall findings of *Swietlicki et al.* [2000] and is also valid for the five cases we analyze here. Second (section 3.1.2), we analyze CCN activation spectra measured on the M-IV and compare those to predicted spectra obtained using the Köhler model. The Köhler model uses as input aerosol size spectra and submicron aerosol chemistry measurements made at the surface site.

3.1.1. Modeled and Observed Growth Factors

[32] Table 4 provides an overview of the Köhler model used in this work. A complete description of the model is provided in Appendix A. In addition to the assumption about the mixing state of the aerosol (section 3.1), the following assumptions are implicit in our approach: (1) a fraction of the particle mass (ε) is composed of water-soluble solute, (2) the insoluble mass has a bulk density equal to 1700 kg/m^3, and (3) dried particles are compact spheres. These assumptions do not specify the chemical make up of the particles, which in addition to the soluble fraction is needed for initializing the Köhler model, so the first objective is to specify a water-soluble material that mimics the observed growth factors. Note that the model assumes that the large mode particles are composed of

Table 4. Initialization of the Köhler Theory and Parcel Models[a]

	Aitken and Accumulation Mode	Large Mode
Aerosol		
Data source	surface site DMA	surface site APS
Dry size range	0.006 to 0.5 μm	0.5 to 4 μm[b]
Composition	$(NH_4)_2SO_4$, or NaCl, and insoluble material (internally mixed)	100% NaCl
	Single Mode	
CNN		
Data source	M-IV CCN and CN data fit to single-mode function [*Ji and Shaw*, 1998]	
Dry size range	0.006 to 4 μm	
Composition	$(NH_4)_2SO_4$, or NaCl, and insoluble material (internally mixed)	

[a]All parcel model calculations were initialized at RH = 95%. The thermal accommodation coefficient and the condensation coefficient were set at 1.0 and 0.1, respectively [*Shaw and Lamb*, 1999].

[b]The upper limit size was calculated as 4 times the product of the large mode median size and the corresponding geometric standard deviation (section 3.2.1).

sodium chloride (NaCl), and that is consistent with the fact that aerosol volume ascribable to the large mode (Figure 2) is reasonably consistent with supermicron NaCl mass measurements (section 2.1.1) and with the predominance of NaCl at supermicrometric sizes as reported by *Quinn et al.* [2000].

[33] Measurements of the aerosol growth factor are shown in Figure 5. These data were collected during the time intervals the M-IV was flying north of the surface site on 26 June and 9 July. At the largest dry sizes the growth factors are ~1.75 and are relatively constant. Over the 0.07 to 0.26 size range the model captures the observed rate of growth factor increase with increasing dry size; however, at dry sizes smaller than 0.07 μm the model overestimates the rate of increase. Comparison of the middle black curve to the data demonstrates that the nominal soluble fraction, plus the assumption that the water-soluble component is NaCl, places an upper bound on the growth factor observations. Results presented in Table 5 show that the growth factor measurements are always smaller than this upper limit. Figure 5 also demonstrates that the nominal soluble fraction, plus the assumption of $(NH_4)_2SO_4$ as the water-soluble component, defines a lower boundary for the growth factor measurements. We conclude that the nominal solubility values, plus thermodynamic property data for either NaCl or $(NH_4)_2SO_4$, lead to predictions that encompass the range of observed growth factor values.

3.1.2. Predicted and Observed CCN Activation Spectra

[34] Using the assumptions stated in the previous section, we now compare predicted CCN activation spectra to airborne measurements made with the CCN instrument. With regard to the prediction it is important to note that these are based on aerosol size spectra measurements performed at the surface site. Those spectra were converted to CCN activation spectra using Köhler theory predictions of the relationship between critical supersaturation and dry diameter (Figure A2). Input into that calculation is the nominal soluble fraction (Table 1). Implicit in the prediction of CCN activation spectra from size spectra is the assumption, validated in section 3.1, that the aerosol is internally mixed.

[35] Figure 6 shows, for the 26 June and 9 July cases, comparisons of the observed and predicted CCN spectra. Note that we express the CCN amount as a mixing ratio (i.e., count per unit mass of air) so that the surface measurements can be compared to those obtained at the lower pressure of the M-IV (~900 versus 1013 hPa). The black and gray curves are predictions based on the assumption that the water-soluble portion of the Aitken and accumulation mode particles is composed of either NaCl (black curve) or $(NH_4)_2SO_4$ (gray curve). Also note that the NaCl curve lies above and to the left of the $(NH_4)_2SO_4$ curve. This is a consequence of the fact that NaCl particles activate at lower critical supersaturation when compared to $(NH_4)_2SO_4$ particles of the same size and soluble fraction. Also shown in Figure 6 are CCN (green squares) and CN (green triangles) measurements from the M-IV. Note that the CN measurements are plotted at the theoretical prediction for 0.01 μm ammonium sulfate particles (S = 6%). We fitted the combined CCN and CN measurements using the unimodal fitting function developed by *Ji and Shaw* [1998]. In fact, a fraction of the particles detected as CN may activate at water supersaturations larger than 6%, but since the fitted spectra usually exhibit a "knee" at supersaturations smaller than 6% (green curve) that assumption is justified. At supersaturations smaller than the "knee" the Ji and Shaw fitting function is consistent with the classical CCN fitting function of the form $N = CS^k$ proposed by *Twomey* [1959]. We employ the function developed by Ji and Shaw because it approximates the expected behavior at large supersaturation while also mimicking the Twomey function a lower supersaturations. Another feature of the Ji and Shaw function its mathematical form which allows for easy calculation of supersaturations corresponding to prescribed fractions of the total mixing ratio. This feature is exploited below in our comparisons of the measured and predicted CCN spectra.

[36] The CCN measurements shown in Figure 6 exhibit considerable variation about the best fit line. We have evaluated the fraction of the variability attributable to statistical error resulting from the small volume sample rate of the CCN instrument. This variability was calculated using Poisson statistics, a CCN sample volume equal to 0.4 cm^{-3} per sample [*Delene et al.*, 1998] and the fact that the CCN instrument processes two samples per minute. The inferred variability is roughly a factor of 2 smaller than that observed. It is therefore reasonable to conclude that a significant fraction of the observed variability is attributable to spatial nonuniformity in the ambient CCN. CN data shown in Figure 6, plus the larger volume sample rate of the CN counter (1500 cm^3/min versus 0.8 cm^3/min),

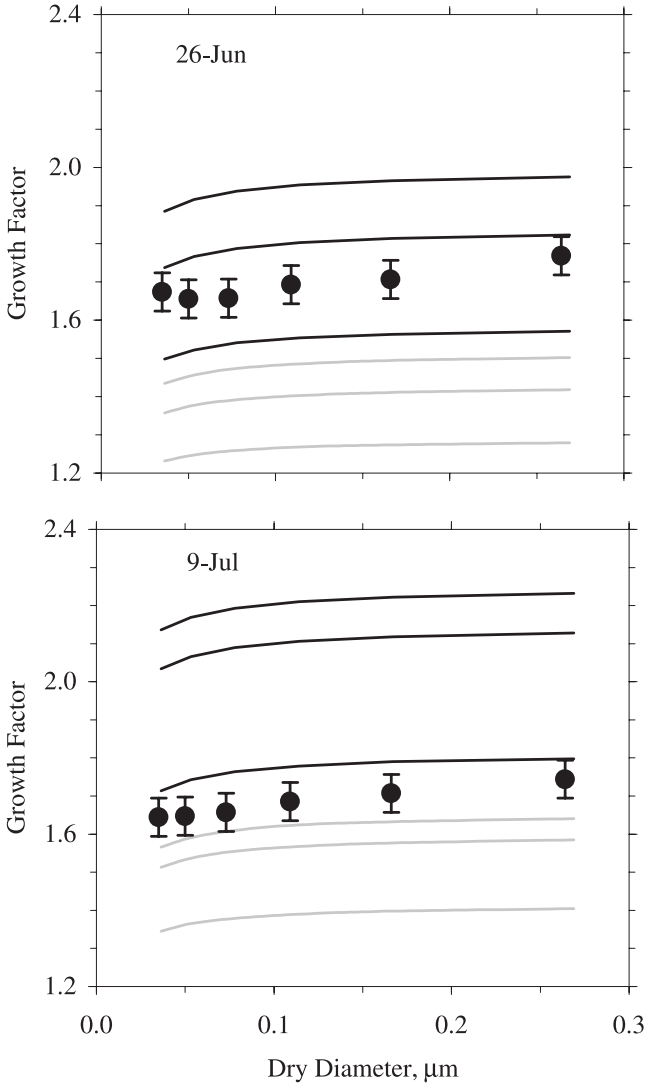

Figure 5. RH = 90% growth factor observations (filled circles) [from *Swietlicki et al.*, 2000], made at the surface site during M-IV flight intervals on 26 June (top) and 9 July (bottom). Predicted growth factors (black and gray lines) are also plotted. The three black lines are Köhler model predictions based on the upper limit, nominal, and lower limit soluble fraction values, each with sodium chloride (NaCl) as the water-soluble component. Köhler model predictions evaluated using the upper limit, nominal, and lower limit soluble fraction values, each with ammonium sulfate ($(NH_4)_2SO_4$) as the water-soluble component, are indicated by gray lines.

Table 5. Growth Factors Corresponding to 0.11 μm Dry Particles[a]

Date	Predicted GF for $(NH_4)_2SO_4$	Predicted GF for NaCl	Observed GF
25 June	1.6	2.1	1.7
26 June	1.4	1.8	1.7
9 July	1.6	2.1	1.7
17 July	1.5	2.0	1.6
18 July	1.6	2.1	1.6

[a]Abbreviation GF is growth factor.

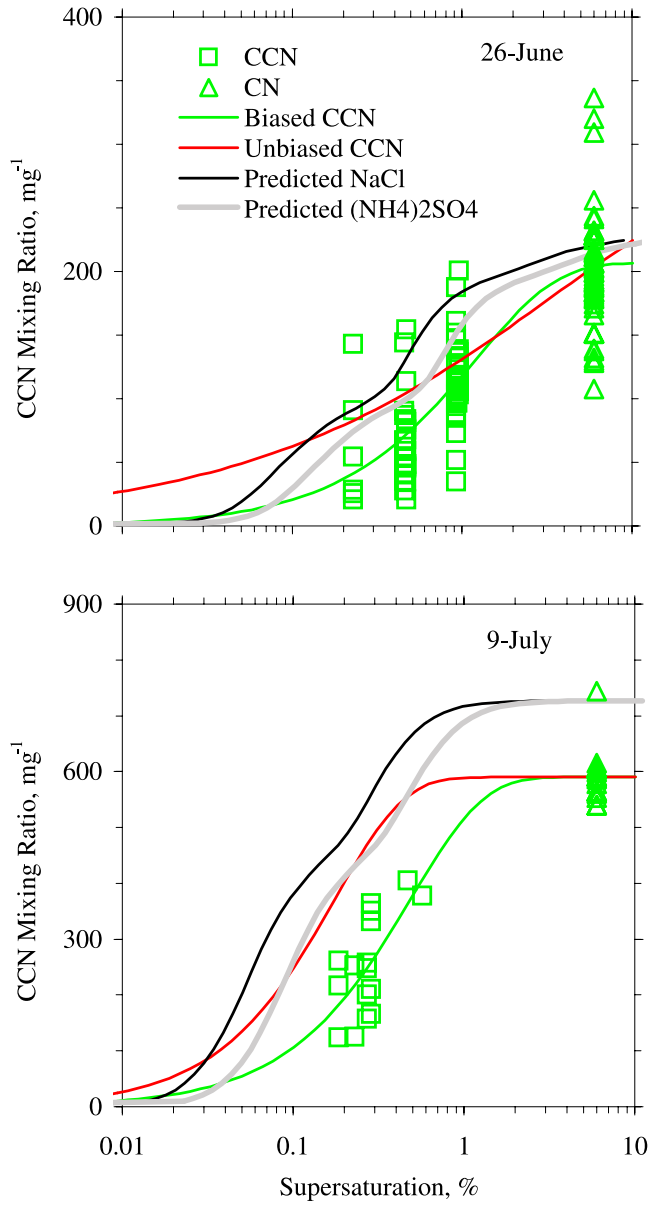

Figure 6. CCN measurements from the UWyo instrument flown on the M-IV. These were combined with the CN measurements and fitted to the function of *Ji and Shaw* [1998]. The fitting function is shown (green line). The CCN data were also unbiased using equations (1), (2), (3), and (4), and refitted (red line). Also illustrated are predicted CCN spectra derived using composited DMA-APS size spectra, nominal soluble mass fraction values and the assumption that the soluble aerosol mass is either ($(NH_4)_2SO_4$) (gray line) or NaCl (black line).

are also indicative of spatial nonuniformity. In part 1 we report vertical profile CN measurements. These show little if any trend in CN with height through boundary layer, particularly for the two cases shown in Figure 6 (26 June and 9 July). Those results, combined with the ±20% agreement between flight-average CN measurements made both at the surface site and on the M-IV (part 1 and section 2.2) and the variability shown in Figure 6, are suggestive of source processes active within the marine boundary layer (e.g., sea spray and entrainment from the free troposphere)

which are continuously in the process of being homogenized by boundary layer turbulence.

[37] Figure 6 shows that the predicted spectra, based on $(NH_4)_2SO_4$ and the nominal soluble fraction (gray line), overpredict mixing ratio values inferred using the fitted CCN data (green line). Furthermore, the disparity is larger when the CCN fit is compared to the prediction based on NaCl and the nominal soluble fraction. After correcting the CCN data for the type-1 and type-2 errors (section 2.3), and refitting, the red curve was obtained. The red curve plots close to the $(NH_4)_2SO_4$ prediction over a substantial range of supersaturation. At low supersaturations ($S < 0.08\%$ on 26 June and $S < 0.03\%$ on 9 July) the unbiased CCN fit overestimates both predictions. The large relative differences at low supersaturation results from the fact that there are no CCN measurements available to constrain the fit, and also from the fact that the aerosol spectra are trimodal (Figure 2) and thus more complex than that assumed when applying the uni-modal *Ji and Shaw* [1998] fitting function. Comparison of Figures 2 and 6 show that the accumulation and large mode particles determine the cumulative mixing ratio where the unbiased CCN fits overestimate the predicted CCN activation spectra. Indeed, if we had used an instrument that is capable of quantifying the CCN in this low supersaturation range, improved consistency between the measurement and prediction would have been expected. Given the inherent limitations of the static thermal gradient diffusion technique at such low supersaturations [*Squires*, 1971] we are forced to base the comparisons on fitted extrapolations of CCN measurements made at larger applied supersaturations ($S \geq 0.2\%$).

[38] Comparisons of predicted and observed CCN were formulated in terms of supersaturations defining 25 and 50% of the total mixing ratio. Results are shown in Figure 7 where we use the color scheme employed in Figure 6. Generally, the biased CCN is characterized by larger 25th percentile (top panel) and the largest 50th percentile supersaturations (bottom panel). Also observe that the 25th percentile supersaturations based on the unbiased CCN data exceed the $(NH_4)_2SO_4$ prediction (18 July), agree with the $(NH_4)_2SO_4$ prediction (26 June and 17 July), fall between the $(NH_4)_2SO_4$ and NaCl predictions (9 July), or is smaller than the NaCl prediction (25 June). With one notable exception (26 June), which is attributable to the shallow slope of the unbiased CCN spectrum seen in Figure 6, the unbiased CCN versus the predicted CCN supersaturation rankings are repeated in the 50th percentile comparison.

[39] Although not used to formulate a predicted CCN activation spectrum for presentation in Figure 6, the effect of correcting the Aitken and accumulation mode sizes by the factor $D_{se}/D_{me} = 0.8$ is shown in Figure 7. Of importance is the fact that the correction does not completely reconcile the biased-CCN and $(NH_4)_2SO_4$-predicted spectra. The largest disparities remain for 17 and 18 July. Those days are classified as polluted based on submicron mass measurements reported in Table 1, and also based on air mass trajectory information presented in part 1. Better consistency is seen for the two unpolluted cases (25 and 26 June), and for the 25th percentile comparison of 9 July.

[40] The CCN comparisons shown in Figure 7 exhibit both reasonable and not so reasonable agreement depending on supersaturation and study day. In the next section we demonstrate how these differences influence the predicted CDNC. The latter are based on the parcel model, initialized with either size spectra measurements made at the surface or with dry size spectra inferred using CCN activation spectra measurements. When employing measured CCN activation spectra, a transformation is made from supersaturation to dry particle size by evoking the relationship provided by Köhler theory (Figure A2). The nominal soluble fraction is a parameter used in that transformation. Most of the parcel model calculations initialized with measured aerosol size spectra are based on the assumption that the soluble mass (at Aiken and accumulation mode sizes) is ammonium sulfate, but we also consider the effect of changing that material to sodium chloride.

3.2. Kinetic Closure

3.2.1. Parcel Model Initialization

[41] A complete description of the parcel model is provided in Appendix A. Table 4 summarizes important aspects of the model and the data used to initialize it. Initialization spectra consist of (1) the *Ji and Shaw* [1998] fit of the biased CCN measurements, (2) the Ji and Shaw fit of the unbiased CCN measurements and (3) the dry size spectra composited from surface measurements made with a DMA and an APS (Figure 2). Particles contributing to these spectra are assumed to be internally mixed. Furthermore, attention is focused on simulations initialized with ammonium sulfate as the soluble salt (at Aiken and accumulation mode sizes). This assumption follows from the fact that growth factor measurements are in better agreement with predictions which assume $(NH_4)_2SO_4$ in combination with the nominal soluble fraction values (Table 5).

[42] The maximum and minimum dry particle sizes simulated by the parcel model are determined by the minimum size detected at the surface site (0.006 μm) and by an upper limit size calculated as four times the product of the large mode median size and geometric standard deviation. A representative value is 4 μm. This stricture was adhered to in model runs initialized with both CCN and aerosol spectra.

[43] Model predicted CDNC values correspond to droplets larger than 2.6 μm (i.e., the minimum size detected by the Fast-FSSP). These were evaluated, in the parcel model, at 69 m above cloud base. We make no distinction between droplets that have exceeded their critical size, and those that have not, in our evaluation of predicted CDNC. All simulations were initialized at RH = 95% and the initial droplet sizes were predicted using Köhler theory.

3.2.2. Quasi-Adiabatic CDNC

[44] Conditionally sampled CDNC measurements are utilized in this section of the analysis. These were obtained from *Pawlowska and Brenguier* [2000], who evaluated data from the Fast-FSSP flown on the M-IV during ACE-2. Conditional sampling of the CDNC is needed since there are processes active in stratocumulus, specifically drizzle formation and the entrainment of dry air from cloud top, that diminish the CDNC produced by CCN activation. Further, neither drizzle formation nor dry air entrainment is accounted for in the parcel model. The sampling procedure developed by Pawlowska and Brenguier considers data collected during the numerous ascending or descending profiles made through the cloud layer. Data from those

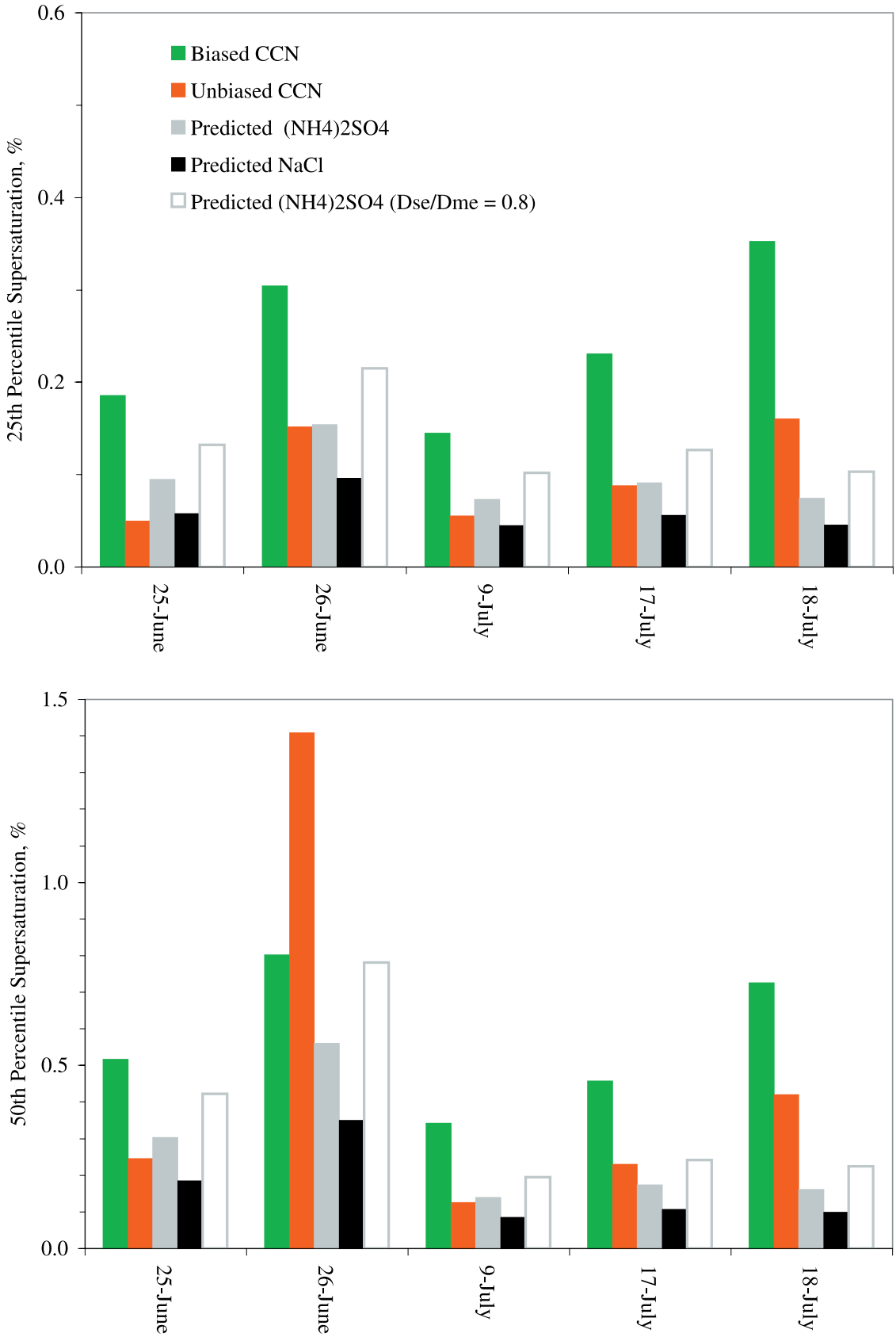

Figure 7. The 25th percentile (top) and 50th percentile (bottom) supersaturations corresponding to the biased and unbiased CCN activation spectra and to CCN activation spectra derived using composited DMA-APS size spectra and the assumption that the soluble aerosol mass is either ($(NH_4)_2SO_4$) or NaCl.

soundings were used to characterize the thermodynamic state at cloud base and to thus select CDNC, conditionally, based on a comparison of the measured and adiabatic cloud liquid water content (LWC) values. The sampling procedure rejects CDNC values from cloud regions having LWC less than 90% of the adiabatic value and drizzle concentrations greater than 2 cm^{-3}. The sampling procedure also rejects data from the lower and upper portions of the cloud soundings since a significant fraction of the droplets there are comparable in size to the minimum diameter detected by the Fast-FSSP (2.6 μm). Pawlowska and Brenguier show that their sampling procedure diminishes the width of the CDNC probability distribution function and that the reduction is most evident at the smallest values of CDNC. They also emphasize that the width of the distribution corresponding to the conditionally sampled CDNC should remain finite since vertical velocity is a varying determinant of the CDNC. Results of the sampling procedure, taken from Table 1 of Pawlowska and Brenguier, are shown as solid horizontal lines in Figure 8. This represents the average of the conditionally sampled CDNC probability distribution function. Also indicated are the averages plus or minus one standard deviation (dashed lines). In the subsequent discussion we refer to the statistics of CDNC derived from the selected cloud regions as the quasi-adiabatic CDNC.

3.2.3. Kinetic Closure

[45] In Figure 8 we compare the quasi-adiabatic CDNC to predictions. Individual graphs are shown for the five study days and a different scale is used for the *y* axis of graphs displaying the two unpolluted cases (0 to 150 cm^{-3}, 25 and 26 June), thus distinguishing them from the three polluted cases (0 to 600 cm^{-3}; 9, 17 and 18 July). The statistics (average and standard deviation) of the predicted CDNC were generated using the truncated vertical velocity probability distribution function (section 2.2.2), and three descriptions of the dry aerosol size spectrum: (1) size spectra based on the biased CCN activation spectrum (green squares), (2) on the unbiased CCN activation spectra (red squares), and (3) composited DMA-APS measurements (gray points). When examining the error bars displayed in Figure 8 it is important to recognize that the indicated variability originates from pdf(w) and is not indicative of experimental error. Figure 8 shows poor consistency between mean values corresponding to the quasi-adiabatic CDNC and those inferred using the composited DMA-APS size spectra measurements. Expressed as a predicted-to-observed CDNC ratio, the disparity is largest for 17 July (2.2) and smallest for the 26 June and 9 July cases (1.5 and 1.4, respectively). In contrast, predicted-to-observed CDNC ratios corresponding to predictions based on the biased CCN data agree within ±30% of the quasi-adiabatic averages. The latter is expected from the work of *Snider and Brenguier* [2000], who used an analytic expression to calculate CDNC as a function of CCN and updraft, and from the fact that the analytic solution and the parcel model prediction agree within 2% (Table A1). Also seen in Figure 8, and in the work of *Snider and Brenguier* [2000], is that the widths of the predicted CDNC probability distribution functions are generally larger than widths corresponding to the distribution of quasi-adiabatic CDNC values. Although we are uncertain of the exact cause of this broadening, we are aware of factors which contribute to it. First, recall that the mean of pdf(w) is forced to 0.0 m/s (section 2.2.2) and therefore larger statistical weighting is associated with the near-zero, but positive, vertical velocity values. Second, we conjecture that parcels moving at speeds just slightly in excess of 0.0 m/s may not persist long enough to make a contribution to CDNC.

[46] Up to this point we have assumed for all dry particle sizes, in the case of the simulations based on CCN, and for the Aitken and accumulation mode sizes in the case of simulations based on the composited DMA-APS size spectra, that the aerosol soluble mass is composed of $(NH_4)_2SO_4$. Furthermore, large mode particles are assumed to be composed of NaCl (Table 4). Changing the soluble composition to NaCl for all particles, but holding the soluble mass fraction constant, increases the predicted mean values of CDNC by approximately 10% (results not shown). Increased availability of activated nuclei when going from the $(NH_4)_2SO_4$ to the NaCl scenarios is the explanation for this behavior. An examination of the black (NaCl) and gray ($(NH_4)_2SO_4$) curves in Figure 6 illustrates this point. This result is somewhat surprising since supersaturation inhibition, due to the presence of the more hygroscopic NaCl nuclei, can in some model simulations reduce CDNC. However, our results indicate that the change from $(NH_4)_2SO_4$ to NaCl results in nuclei availability dominating over the effect of parcel supersaturation inhibition. The insensitivity of predicted CDNC values to the CCN data correction (i.e., equations (1), (2), (3) and (4)) is also indicative of these competing effects. In the comparison of CDNC predictions resulting from the fits of the unbiased and the biased CCN data (Figure 8) supersaturation inhibition negates a portion of the expected CDNC increase. For this comparison particle composition is fixed, but the nuclei count is enhanced, particularly at low supersaturations (Figure 6), as is expected since the CCN data corrections are largest at low supersaturation.

3.2.4. Aerosol Mass

[47] As was discussed previously, *Putaud et al.* [2000] performed measurements of aerosol mass at sizes smaller than the dry cut diameter shown in Figure 2 (0.85 μm). Their measurements, shown in the second column of Table 6, combined with masses obtained by integrating either size spectra (Figure 2) or CCN activation spectra (Figure 6), facilitate data validation independent of the CCN and CDNC comparisons already discussed. This validation is especially relevant since we are questioning the $D_{me} = D_{se}$ assumption which is the basis for the type-2 CCN correction.

[48] When examining the predicted-to-observed mass ratios (Table 6) it is important to recognize the limitations of the mass measurement and thus limitations in the comparison of the mass values. Chemically derived mass measurements, corresponding to submicron aerosol samples collected at the surface, are used in this comparison [*Putaud et al.*, 2000]. These measurements were made with a precision of ±40% (section 2.1.2). However, in the comparison even larger relative error is expected because the model-initializing aerosol and CCN spectra are flight-interval averages (1 to 4 hours) while the filter measurements are 11 hour averages. Predicted-to-observed mass ratios between 0.5 and 2 are taken to be acceptable in the following comparison. The values presented in Table 6 reveal the

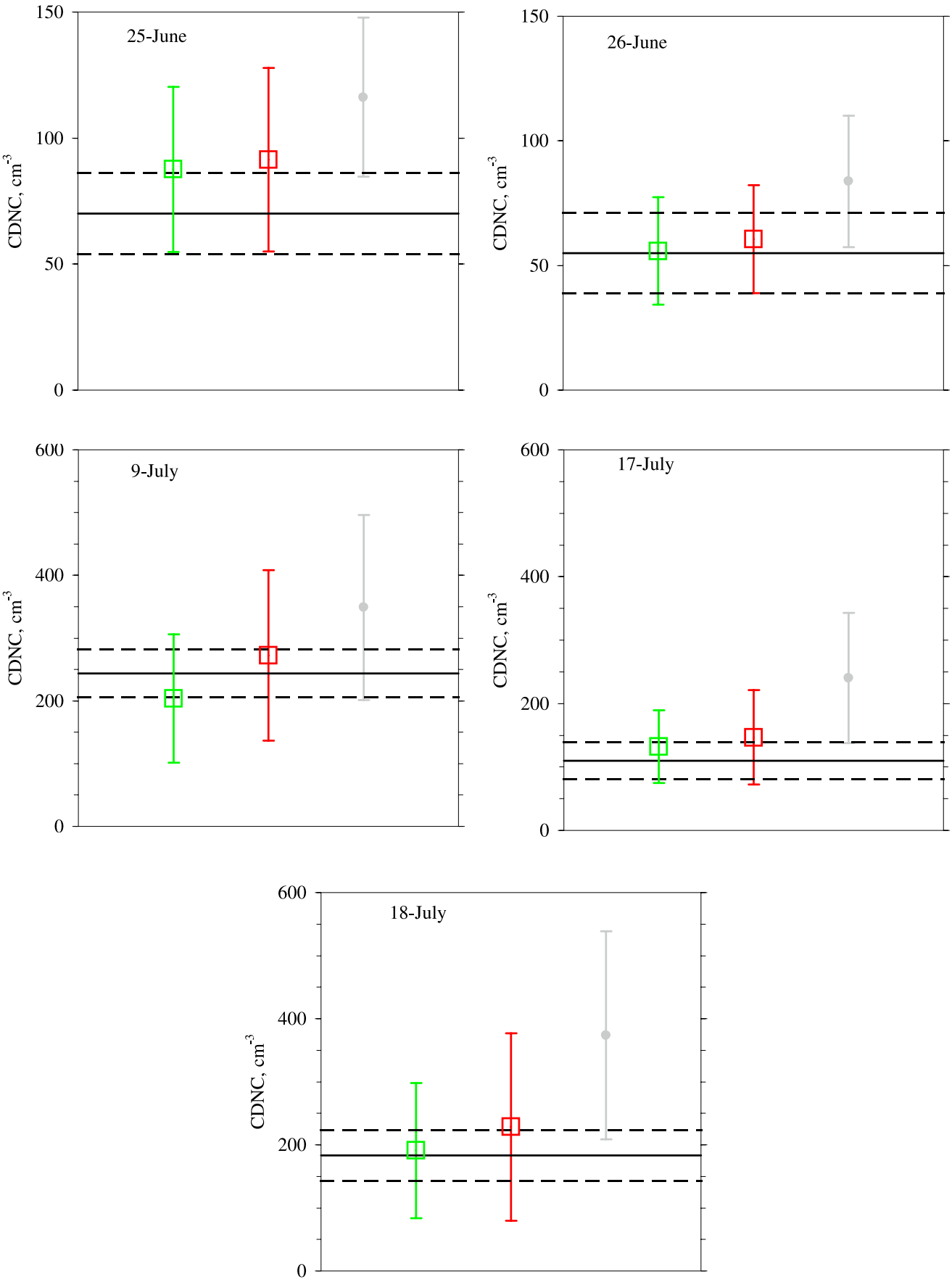
25-June
26-June
9-July
17-July
18-July
CDNC, cm-3
0
50
100
150
200
400
600

Table 6. Predicted-to-Observed Submicron Aerosol Mass Ratios

Date	Observed Submicron Mass, μg/m^3	Predicted-to-Observed Submicron Aerosol Mass Ratios				
		Aerosol				
		Condition 1[a]	Condition 2[b]	Condition 3[c]	Biased CCN	Unbiased CCN
25 June 1997	0.7	1.3	2.0	1.3	3.1	7.8
26 June 1997	1.2	0.7	0.9	0.6	1.2	3.4
9 July 1997	5.8	0.9	1.1	0.7	1.0	2.4
17 July 1997	3.4	1.0	1.3	0.8	0.7	2.6
18 July 1997	5.9	1.2	1.5	1.0	0.4	1.5

[a]Condition 1 corresponds to no large mode, and D_{se}/D_{me} = 1.0 for the Aitken and accumulation modes.
[b]Condition 2 corresponds to inclusion of the large mode, up to D = 0.85 μm, and D_{se}/D_{me} = 1.0 for the Aitken and accumulation modes.
[c]Condition 3 corresponds to inclusion of the large mode, up to D = 0.85 μm, and D_{se}/D_{me} = 0.8 for the Aitken and accumulation modes.

following: (1) Spectrally integrated mass values obtained from the composited DMA-APS size spectra after applying the D_{se}/D_{me} = 0.8 correction to the Aitken and accumulation mode measurements (both made with a DMA), are consistent with the chemical mass measurement (column 5). (2) With the exception of 25 June, and possibly 18 July, mass values derived from the biased CCN spectra are also consistent with the chemical mass measurement (column 6). (3) With the possible exception of 18 July, mass values derived using the unbiased CCN spectra overestimate the chemical mass measurements (column 7). The first inference leaves open the possibility that the CDNC overestimation seen in Figure 8 stems from aerosol oversizing, relative to the actual sphere equivalent diameters. The second and third inferences reinforce our suspicion that the type-2 CCN error (Figure 4) can be attributed to bias in the selection of particle mass coming from the incorrect assumption that $D_{me} = D_{se}$.

4. Discussion

4.1. Model Sensitivity

[49] Plausible explanations for the overestimation of CDNC when using the composited DMA-APS size spectra in the parcel model were investigated by conducting a series of model sensitivity studies. These sensitivity studies show the following:

[50] 1. A factor of 3 reduction in ε (i.e., nominal soluble fraction divided by 3) is needed to reconcile the predicted and observed values of CDNC. Such extreme values of ε are substantially smaller than the lower limit estimates (Table 1) and also contradict the mass closure reported by *Putaud et al.* [2000]. In that case, the observed hygroscopic growth factors would also be inconsistent with predictions based on the Köhler theory model. This is evident from consideration of Figure 5 and Table 5.

[51] 2. Also explored was the possibility that the maximum supersaturation predicted by the parcel model, and hence the predicted CDNC, are overestimated because of an underestimation of the large aerosol mode. As a point of reference note that CDNC averages, based on the parcel model, are relatively insensitive to the inclusion of the large mode in the calculation. This result is shown in the third and fourth columns of Table 7. The sensitivity studies show that enhanced large mode concentrations, at least a factor of three larger than that indicated by the APS, combined with enhanced large mode geometric standard deviations, at least a factor 1.5 larger than that also indicated by the APS, are needed to explain the CDNC overestimation. These inferred large mode parameters are not only unrealistic compared to the climatology reported by *Gras* [1995], but they also imply a supermicrometric aerosol mass that is roughly two orders of magnitude larger than the observed by *Quinn et al.* [2000] during ACE-2.

[52] 3. Also evaluated was sensitivity to the $D_{me} = D_{se}$ assumption. Critique of this assumption is justified by laboratory measurements (Table 3), by the mass consistency reported in the fifth column of Table 6, and by the fact that observed growth factors are relatively insensitive to the mobility equivalent size (Figure 5). Predicted-to-observed CDNC ratios reported in the fourth and fifth columns of Table 7 show that the D_{se}/D_{me} = 0.8 correction produces only a small (<15%) reduction of that ratio.

4.2. Sensitivity to Vertical Velocity

[53] Bias in the measured vertical velocities was also investigated as a plausible explanation for the CDNC overestimation. In Figure 9 we infer what the vertical velocity statistics would need to be to bring closure between the prediction and observation of CDNC. These results were obtained by inputting quasi-adiabatic CDNC averages, and the mean quasi-adiabatic CDNC plus or minus 1 standard deviation, into the relationship between CDNC and vertical velocity (Figure A1). The methodology is shown in Figure 1d. As was the case in Figure 8, the error bars shown in Figure 9 indicate the mean of the inferred pdf(w) plus or minus one standard deviation. Note that the predicted vertical velocities are substantially smaller than the observations.

[54] Since other investigators have measured the width of the pdf(w) it is interesting to compare the values presented here to those other results and to thus investigate the possibility of a bias in the vertical velocity measurements obtained from the M-IV gust probe. For this assessment we compare standard deviations of the complete vertical veloc-

Figure 8. (opposite) Mean cloud droplet number concentration (CDNC) predicted by the parcel model initialized with dry size spectra derived using biased CCN spectra (green squares), unbiased CCN spectra (red squares) and composited DMA-APS size spectra (gray points). Error bars indicate the width (1 standard deviation) of the predicted CDNC probability distribution function. Horizontal lines show the average and the average plus or minus 1 standard deviation of the conditionally sampled CDNC probability density function [*Pawlowska and Brengier*, 2000].

Table 7. Predicted-to-Observed CDNC Ratios

Date	Observed CDNC, cm^{-3}	Predicted-to-Observed CDNC Ratios				
		Aerosol				
		Condition 1[a]	Condition 2[b]	Condition 3[c]	Biased CCN	Unbiased CCN
25 June 1997	70	1.7	1.7	1.5	1.3	1.3
26 June 1997	55	1.5	1.5	1.3	1.0	1.1
9 July 1997	244	1.6	1.4	1.4	0.8	1.1
17 July 1997	110	2.4	2.2	1.9	1.2	1.3
18 July 1997	183	2.2	2.0	1.9	1.0	1.2

[a]Condition 1 corresponds to no large mode, and $D_{se}/D_{me} = 1.0$ for the Aitken and accumulation modes.
[b]Condition 2 corresponds to inclusion of the large mode, and $D_{se}/D_{me} = 1.0$ for the Aitken and accumulation modes.
[c]Condition 3 corresponds to inclusion of the large mode, and $D_{se}/D_{me} = 0.8$ for the Aitken and accumulation modes.

ity probability distribution functions, not those derived from the truncated distributions. The range of values reported by *Boers et al.* [1998], in their analysis of airborne gust probe data from marine stratocumulus clouds are in good agreement with the range of values we report in section 2.2.2. There is also consistency with the parameterizations of *VanZanten et al.* [1999], who conducted numerical studies of turbulence in a cloud-topped boundary layer. Both results lend support to the assertion that the values of w recorded by the M-IV are consistent with current understanding of vertical velocity in stratocumulus and discount the conjecture that the CDNC overestimate is explicable in terms of positive bias in the measurement of vertical velocity.

4.3. CDNC Measurement Uncertainty

[55] Negative bias in the measurement of CDNC may also explain the CDNC overestimation. For reasons discussed in section 2.2.1 we are confident that study days exhibiting the largest CDNC overestimations (17 and 18 July), factors other than CDNC measurement bias must be at work. In contrast, CDNC predictions from 26 June and 9 July are reasonably consistent with the observations. For these cases, and particularly for the 26 June case, the degree of consistency is improved if the composited DMA-APS size spectra are modified by the $D_{se}/D_{me} = 0.8$ correction (Table 7). After applying that correction, the observed-to-predicted CDNC ratio is 1.3 and thus the predicted CDNC value falls within an error band defined by uncertainty in the CDNC measurement (section 2.2.1). Less improvement was found for the 9 July case, but even without the $D_{se}/D_{me} = 0.8$ correction the predicted CDNC value lies within the CDNC error band.

4.4. Summary

[56] In the preceding sections, several rationalizations for the CDNC overestimation were explored. We have examined sensitivity to error in the following parameters: (1) submicron aerosol water-soluble mass fraction, (2) large mode aerosol number concentration and spectral width, (3) dry particle size classified by differential mobility analyzers, both in the laboratory and in the field, (4) vertical velocity, and (5) CDNC. Taken separately, none of these uncertainties can account for the CDNC overestimation. Complicating this is the fact that the static closure result, while suggesting plausible ways to reconcile the incongruous CCN and DMA measurements, is inconclusive. It does indicate that the predicted and observed CCN can be reconciled by applying the CCN data corrections (i.e., equations (1), (2), (3) and (4)), but leaves open the possibility that the type-2 CCN error (i.e., equations (3) and (4)) may originate from the $D_{me} = D_{se}$ assumption rather than from an overestimation of the applied supersaturation. Evidence corroborating the $D_{se}/D_{me} < 1$ hypothesis comes from laboratory experiments (Table 3) and from comparisons of predicted and observed submicron aerosol mass loadings (Table 6). The latter show that size spectra derived from the biased CCN activation spectra generally reproduce the mass observations while the size spectra corresponding to the unbiased CCN activation spectra overestimate it. Further, we show improved kinetic closure results when D_{se}/D_{me} is set to 0.8 (i.e., the minimum value observed in the laboratory (Table 3)). This correction moves the CDNC prediction to within the uncertainties associated solely with the CDNC measurement on two days (26 June and 9 July; Table 7). Outstanding is the problem of explaining the lack of kinetic closure on one unpolluted day (25 June) and on two days influenced by continental pollution (17 and 18 July).

[57] The 25 June case is exceptional since both the composited DMA-APS size spectrum and the CCN-based size spectrum lead to overestimation of the quasi-adiabatic CDNC (Figure 8). However, the predicted-to-observed CDNC ratios (1.5 and 1.3; Table 7) are relatively close to unity and these could be indicative of measurement error associated with CDNC, CCN, aerosol or vertical velocity. In addition, the surface data averaging interval was shortest on 25 June (50 min, section 2.1.1), so we cannot completely rule out the possibility that aerosol spatial nonuniformity contributed to the lack of closure on 25 June. The fact that the predicted-to-observed submicron mass ratio, based on the CCN, is larger than unity (Table 6, sixth column)

Figure 9. (opposite) Vertical velocity predicted by inputting CDNC mean values, and CDNC mean values plus or minus one standard deviation, both from *Pawlowska and Brengier* [2000], into parcel model predictions of the relationship between vertical velocity and CDNC (Figure A1). Results corresponding to model runs made with biased CCN, unbiased CCN, and composited DMA-APS size spectra, are indicated by green squares, red squares, and gray points, respectively. Horizontal lines show the average, the 15th percentile value, and the 85th percentile values corresponding to the truncated vertical velocity probability distribution function.

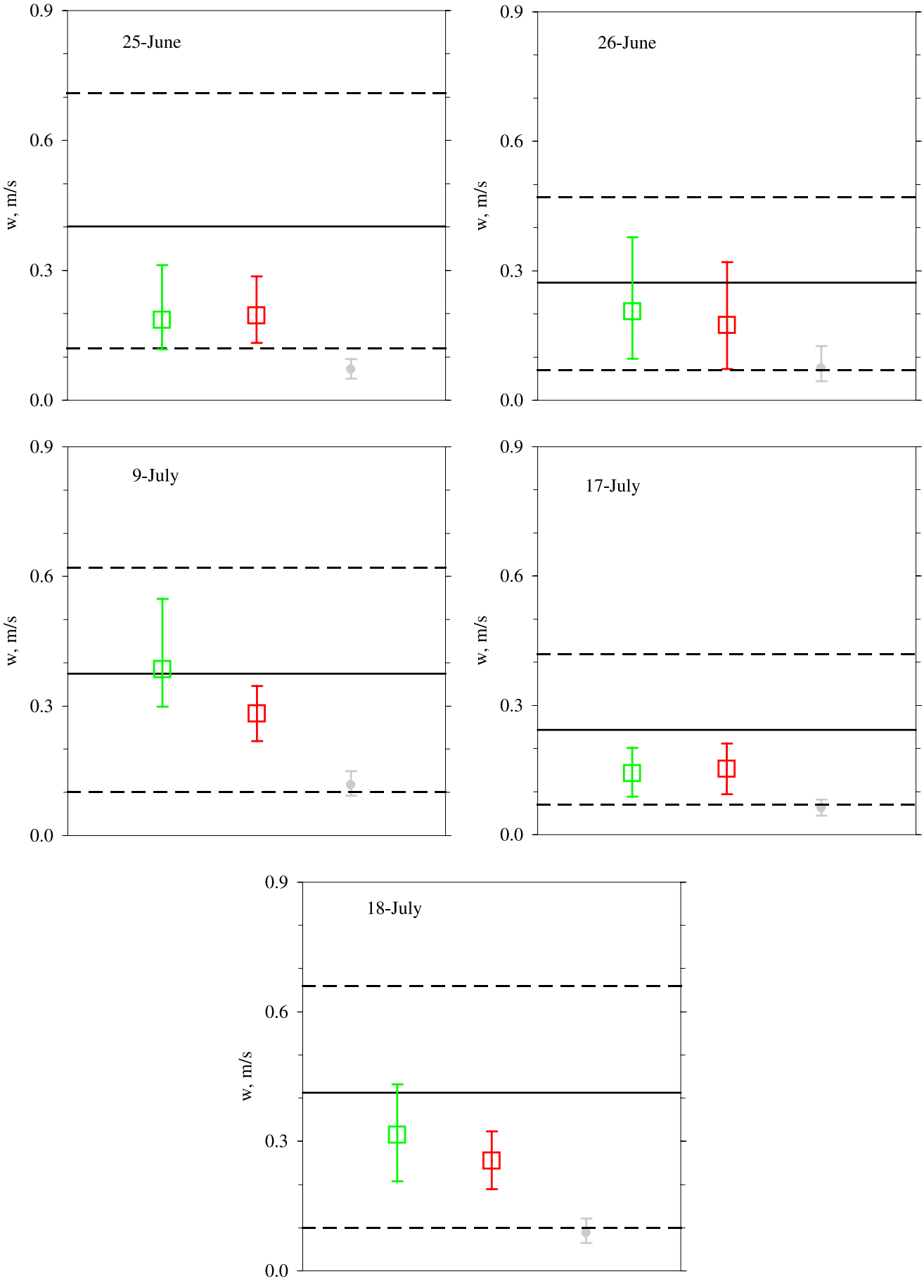
25-June
26-June
9-July
17-July
18-July
w, m/s
0.0
0.3
0.6
0.9

corroborates this suspicion, but it is important to realize that the predicted mass is sensitive to the assumption that the extrapolated uni-modal CCN fit provides an accurate representation of the actual aerosol mass spectrum. Clearly, this assumption is not correct for the dry size spectrum derived using the unbiased CCN since the corresponding predicted-to-observed mass ratio is very large, particularly for the 25 June case. This result is shown in the seventh column of Table 6. A result arguing against spatial nonuniformity as an explanation for the disparity on 25 June is the consistency seen between M-IV and surface site CN concentrations (part 1); however, there are no airborne accumulation mode aerosol measurements available on 25 June to confirm if the observed CN consistency extends to larger particle size.

[58] In contrast to 25 June, the predicted-to-observed submicron mass ratios (sixth column of Table 6) are less than unity on 18 July. Again, this may imply that the surface site aerosol data is not representative of the region of the marine boundary layer sampled by the M-IV but this conclusion is not corroborated by the CN and accumulation mode comparisons presented in part 1. In spite of this, in part 1 we do document a disparity between dry size spectra measured at the surface site and that measured by the CIRPAS Pelican which was coordinated with the M-IV on 18 July. Examination of this case by *Guibert* [2002] has shown that the disparity can produce a 15% overestimation of CDNC when using the surface site aerosol size spectrum (as we have done here) compared to that reported by the Pelican. On 17 July the M-IV flew solo so there is no independent check of the representativeness of the surface site size spectrum measurements; however, CN measurements made on the M-IV do agree with the surface value (part 1). We are therefore reasonably confident that spatial nonuniformity on 17 and 18 July is not a dominant factor in the CDNC closure disparities, but we cannot completely rule it out.

[59] Having attenuated the possibility of a single explanation for the CDNC overestimation, particularly on 17 and 18 July, it is apparent that the disparity we document is either attributable to additive experimental biases or to an actual atmospheric phenomenon. With regard to the latter, one possibility is that the theoretical hypothesis linking maximum parcel supersaturation and CDNC is violated so that only a fraction of the nuclei postulated to act as CCN do actually grow to sizes detectable by the Fast-FSSP or by the CCN instrument. The activation model of *Feingold and Chuang* [2002] does break the supersaturation/CDNC link. That occurs because a film-forming compound, distributed as a function of the initial particle size in a manner consistent with the aerosol surface area spectrum, inhibits the growth of nascent water droplets and particularly those that activate at supersaturations close to the maximum parcel supersaturation. Implicit in their calculations is the assumption that the water condensation coefficient is 10^{-5} if at least a molecular layer of film-forming compound is present on the droplet surface. A consequence is that predicted CDNC values are reduced by as much as a factor of two relative to parcel model calculations which do not consider the hypothesized action of film-forming compounds. Whether or not such compounds exist in the atmosphere, and are distributed as a function of size as envisioned by *Feingold and Chuang* [2002], remains an open question. Consistent with their growth inhibition hypothesis is the observation of submicron organic aerosol mass during ACE-2 [*Putaud et al.*, 2000]; however, that material was not speciated nor is there information on the types of organic compounds that would act in the manner envisioned by Feingold and Chuang. The presence of organic material may also alter the Kelvin and solute effects in the manner modeled by *Shulman et al.* [1996]. Since we assumed that the organic mass fraction is insoluble (section 2.1.3), and not surface active, predictions of CDNC or CCN based on a model that simulates the phenomena discussed by Shulman et al. will be larger than that we report here. If that is the case then the reported discrepancy between prediction and observation will be larger than that shown in Figures 7 and 8, or in Table 7.

5. Conclusions

[60] Our results extend those obtained by previous investigators who considered data sets comprised of aerosol physicochemical properties and CCN [*Fitzgerald*, 1973; *Bigg*, 1986; *Quinn et al.*, 1993; *Covert et al.*, 1998; *Chuang et al.*, 2000; *Wood et al.*, 2000; *Cantrell et al.*, 2001; *Zhou et al.*, 2001] or CDNC and aerosol physicochemical properties [*Hallberg et al.*, 1997, 1998]. The two types of comparisons probed are referred to as the static and kinetic closure studies. In the static closure we show that aerosol physicochemical property data, when used to initialize a Köhler theory model, produces a substantial overestimation of the CCN concentration. This overestimation is reduced if the aerosol size spectra, measured by a DMA, are adjusted to smaller size by accounting for the fact that the mobility equivalent diameter is generally larger than the sphere equivalent diameter. The inference is that bias can occur in static closure studies because aerosol are either nonspherical, porous or are contaminated by water even when they are size classified at a RH which is less than the efflorescence humidity [*Weiss and Ewing*, 1999].

[61] In the kinetic closure study we show that CDNC values derived using aerosol physicochemical property data overestimate quasi-adiabatic CDNC observations. However, CDNC values based on the measured CCN are consistent with the quasi-adiabatic CDNC observations. The CDNC overestimation that occurs when using aerosol physicochemical property data is reduced by shifting the Aiken and accumulation mode particles to smaller size, as in the static closure study, but substantial discrepancies still exist, especially for two of three cases impacted by continental pollution. The discrepancy we document is consistent with models that vary the condensation coefficient as a function of dry particle size and thus predict reductions in cloud droplet concentration [*Feingold and Chuang*, 2002]. It is not reconciled by models which enhance CCN activity and thus predict larger CDNC via the action of organic materials on the Kelvin and solute effects.

Appendix A

[62] A cloud parcel model (referred to as the UWyo parcel model; available at http://www.das.uwyo.edu/ccp/web) is used to predict CDNC as a function of vertical velocity (w). The key model assumption is closed/adiabatic

ascent at a constant vertical velocity. With regard to the properties of the dry particles (Table 4), they are assumed to be compact spheres and their water-soluble mass fraction (ε) is assumed to be the same for all particles of a given size.

A1. Parcel Model Physics and Chemistry

[63] Using the form of the Köhler equation developed by *Chýlek and Wong* [1998], the saturation ratio at the air/solution interface is described using

$$\hat{S}_k = a_{w,k} \cdot \exp\left(\frac{4\sigma_k M_w}{\rho_k R T D_k}\right) \tag{A1}$$

where the subscript (k) tracks the size of the nucleus, $a_{w,\,k}$ is water activity, σ_k is surface tension, D_k is particle diameter, ρ_k is solution density, T is absolute temperature, R is the universal gas constant and M_w is the molecular weight of water.

[64] In equation (A1) the solution composition dependence of surface tension is described using a linear coefficient (Ω) derived from analyses of laboratory data corresponding to the $(NH4)_2SO_4$-water and NaCl-water systems [*Seinfeld and Pandis*, 1998].

$$\sigma_k = \sigma_o + \Omega \cdot m_k \tag{A2}$$

Here σ_o is the pure water surface tension (temperature-dependent) and m_k is the salt solution molality.

[65] Laboratory data are used to describe the salt weight-fraction (x_k) dependence of $a_{w,k}$ and ρ_k.

$$a_{w,k} = 1. + \sum_{i=1}^{i=4} c_i \cdot x_k^i \tag{A3}$$

$$\rho_k = 997.1 + \sum_{i=1}^{i=4} a_i \cdot x_k^i \tag{A4}$$

In equations (A3) and (A4) the fitting coefficients, c_i and a_i, were obtained from *Tang* [1996] and *Tang and Munkelwitz* [1994]. Further, note that the solution composition variables (salt molality and weight fraction) are different in equations (A2), (A3) and (A4). These are related by the equation

$$x_k = \frac{m_k \cdot M_s}{1. + m_k \cdot M_s} \tag{A5}$$

where M_s is the molecular weight of the hygroscopic salt (i.e., ammonium sulfate or sodium chloride). The temperature used in equations (A1) and (A2) is held constant at the temperature corresponding to the laboratory measurements of *Tang* [1996] and *Tang and Munkelwitz* [1994] (298.15 K).

[66] Also employed is a relationship between dry particle volume ($(4\pi/3)D_{d,k}^3$), the volume of the salt contained within the nucleus ($(4\pi/3)D_{s,k}^3$), the water-soluble mass fraction (ε), and the bulk densities of the water-insoluble (ρ_{in}) and water-soluble (ρ_s) material.

$$D_{s,k}^3 = D_{d,k}^3 \Big/ \left(\frac{\rho_s \cdot (1. - \varepsilon)}{\rho_{in} \cdot \varepsilon} + 1.\right) \tag{A6}$$

ρ_{in} is assumed to be 1700 kg/m^3.

[67] Three coupled equations ((A7), (A8) and (A9); discussed below) control the temporal evolution of the parcel thermodynamic and microphysical properties. The thermodynamic energy equation has the form

$$\Delta T = -\frac{(1. + r_v + r_l) \cdot g \cdot w \cdot \Delta t + l_v \cdot \Delta r_v}{c_p} \tag{A7}$$

Here ΔT is the temperature increment corresponding to the model time step Δt, r_v and r_l are the vapor and liquid mixing ratios, g is the acceleration due to gravity, w is the updraft speed, l_v is the latent heat of vaporization, Δr_v is the vapor mixing ratio increment and c_p is the isobaric specific heat capacity. The vapor mixing ratio increment is computed as

$$\Delta r_v = -\left\{\left(\frac{\pi}{6} v \sum n_j \cdot (1 - x_j) \cdot \rho_j \cdot \left(D_j^3 - D_{j,in}^3\right)\right) - r_{l,pre}\right\} \tag{A8}$$

where v is the parcel volume corresponding to a unit mass of dry air, the subscript "j" indicates a particle size bin, n_j is the particle concentration, x_j is the salt weight fraction in the solution phase, ρ_j is the solution density, D_j and $D_{j,in}$ are the sizes corresponding to the complete particle and its insoluble core, and $r_{l,pre}$ is the liquid water mixing ratio evaluated at the previous time step. The parameters x_j, ρ_j and D_j are taken to be the arithmetic average of values at the adjacent bin boundaries.

[68] Droplet growth is described using the equation developed by *Zou and Fukuta* [1999]. This has the form

$$D_k = \frac{\Delta t \cdot \left(\hat{S} - \hat{S}_k\right) \cdot \Psi_k}{D_{k,pre}} + D_{k,pre} \tag{A9}$$

where $D_{k,\,pre}$ is the particle diameter from the previous time step, $\hat{S}$ and $\hat{S}_k$ are the ambient and particle saturation ratios, the latter being described by (A1), and Ψ_k is a coefficient that varies with particle size, temperature, pressure and the condensation and thermal accommodation coefficients (equation (4) from *Zou and Fukuta* [1999]). Unless stated otherwise, the thermal accommodation coefficient and the condensation coefficient were taken to be 1.0 and 0.1, respectively. These values are at the upper limit of the range of values observed by *Shaw and Lamb* [1999].

A2. Model Initialization

[69] Model input dry size spectra were either composited from DMA and APS measurements (Figure 2), or were inferred using CCN activation spectra measured on the M-IV (Figure 6). Table 4 summarizes the range of dry sizes simulated and the particle compositions. At dry sizes smaller than 0.50 μm bin boundaries were specified by a constant diameter ratio ($D_{d,k\,+\,1}/D_{d,k} = 1.09$). The water-soluble aerosol volume is calculated using equation (A6) and prescribed values of D_d and ε. When initializing the model with CCN activation spectra the independent variable is the applied supersaturation. This is converted to D_d via the Köhler relationship between critical supersaturation, D_d and ε. Our formulation of Köhler theory is compared to other published results in section A6.

[70] A reference thermodynamic state was defined by M-IV measurements of temperature and pressure at cloud base. The cloud base state was extrapolated to RH = 95% via a thermodynamic path (assuming a closed parcel boundary and conservation of entropy), thus fixing the

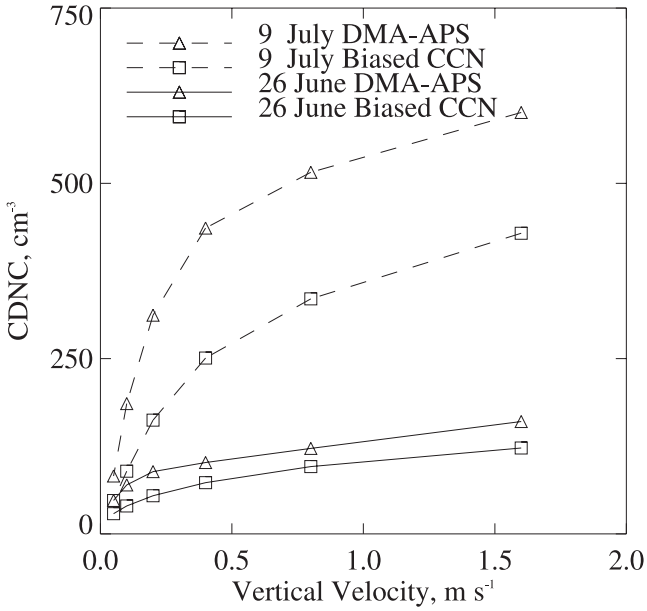

Figure A1. Parcel model calculations of CDNC at vertical velocity equal to 0.05, 0.10, 0.20, 0.40, 0.80 and 1.60 m/s.

starting state at ~100 m below the cloud base. Particle size at the starting state was initialized as the size predicted by equation (A1).

A3. Numerics

[71] The numerical scheme consists of two loops. The outer loop tracks the thermodynamic state of the parcel. This is done by integration of three equations: (1) the thermodynamic energy equation (equation (A7)), (2) the hydrostatic equation, and (3) a water mass balance equation. A time step of 0.1 s is utilized. The inner loop integrates the growth equation (A9) and updates the particle size-dependent properties (m_k, x_k, ψ_k, $\hat{S}_k$, σ_k, ρ_k and $a_{w,k}$) every 0.01 s. Because of numerical instability at the smallest particle sizes [*Fitzgerald*, 1974], two characteristic times are evaluated before applying equation (A9). These characteristic times are discussed by *Chuang et al.* [1997]. The first is defined as the characteristic time associated with equilibrium growth along the Köhler curve ($\tau_{e,k}$). The second is the characteristic time associated with kinetically limited growth. The latter is evaluated using the growth equation (A9) and is symbolized by $\tau_{g,k}$. Particles satisfying the condition $\tau_{e,k} > \tau_{g,k}$, and also smaller than their critical size, are allowed to grow as predicted by the Köhler equation (A1). Growth of all other particles is evaluated using equation (A9).

A4. CDNC Versus *w*

[72] Figure A1 illustrates model output for the 26 June and 9 July 1997 ACE-2 cases. Values of CDNC at the measured values of *w*, based on the M-IV gust probe data, were calculated by linear interpolation among the model-derived points.

A5. Comparison to Other Formulations of Köhler Theory

[73] *Chýlek and Wong* [1998] discuss disparities between different formulations of Köhler theory. Because of the concerns they raise we compared our formulation of Köhler theory to the work of *Fitzgerald* [1973] and *Hoppel* [1979] (Figure A2). Observe that our calculation and the result of Fitzgerald compare very well both for pure ammonium sulfate ($\varepsilon = 1.$) and for particles comprised of ammonium sulfate and insoluble matter ($\varepsilon = 0.1$). This agreement is surprising since *Fitzgerald* [1973] approximates the solute effect, when assuming that the van't Hoff factor (i) is a constant, while our formulation calculates water activity directly and without making any assumption about the van't Hoff factor. However, an examination of Figure 2 of *Young and Warren* [1992] shows that the value of i picked by *Fitzgerald* [1973] (i = 2.4) is a reasonable approximation for droplets that originate on dry particles smaller than ~0.15 μm [*Fitzgerald*, 1975]. Our result is also compared to the approximate Köhler model developed by *Hoppel* [1979]. That treatment assumes $i = 3$ and plots about 15% below our result. This is evident both for pure ammonium sulfate particles and for ammonium sulfate internally mixed with insoluble mass (i.e., $\varepsilon = 0.1$ in Figure A2). We also note that Fitzgerald's $i = 2.4$ assumption is implicit in the work of *Gerber et al.* [1977] and that the latter is commonly referenced as showing experimental validation of Köhler

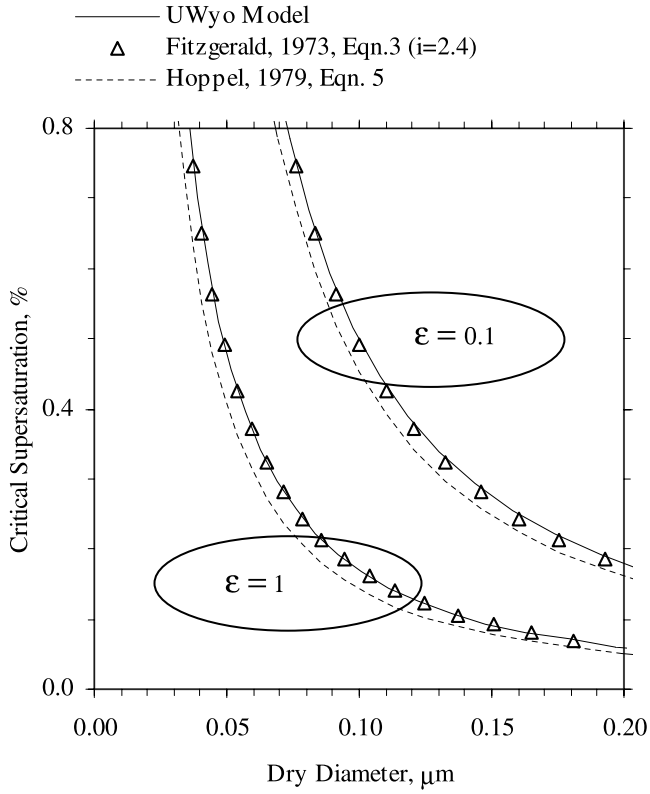

Figure A2. Comparisons of the relationship between critical supersaturation and dry diameter for ammonium sulfate. These predictions are based on different formulations of Köhler theory. Note that the equation developed by *Fitzgerald* [1973] agrees well with the UWyo model prediction (i.e., equations (A1)–(A6)). The calculation is shown for two different values of soluble fraction (1 and 0.1).

theory for $(NH4)_2SO_4$ aerosols [*Pruppacher and Klett*, 1997].

A6. Comparison to Other Parcel Models

[74] Here, CDNC output by the UWyo parcel model are compared to the work of *Young* [1993] and to predictions based on the analytic equation developed by *Twomey* [1959]. For the latter we use the equation developed by *Johnson* [1981] since it incorporates the same assumptions as *Twomey* [1959] but casts the problem in terms of a more conventional independent variable (ambient vapor supersaturation) as opposed to that used by Twomey (dew point elevation). The Twomey model differs from both the UWyo parcel model and the approach of *Young* [1993] in two fundamental ways: (1) it is an analytic solution to the condensational growth equation whereas the other two require numerical integration, and (2) it presumes that the classical diffusion coefficient adequately describes cloud droplet growth [*Johnson*, 1981]. Since imperfect vapor accommodation at the droplet surface reduces the effective diffusivity relative to the classical value, the numerically calculated CDNC is expected to converge with the Twomey model prediction as the condensation coefficient approaches unity.

[75] Comparisons of the calculated values of CDNC are shown in Table A1. Comparisons between the *Young* [1993] and the UWyo models are only possible for one value of the condensation coefficient (0.03). Relative differences are 10 and 17% for the maritime and continental scenarios, respectively. The UWyo model produced smaller values of CDNC for both situations. This is attributed to the different approaches used to describe the Köhler theory in the UWyo model compared to the *Young* [1993] model. Discussion of this issue is given by *Chýlek and Wong* [1998] and *Young* [1993]. Predictions of the UWyo model exceed the Twomey model when the former is initialized using a condensation coefficient smaller than ~0.09. For larger values of the condensation coefficient the UWyo model converges to within 2% of the value predicted by the Twomey model.

Table A1. UWyo Model, *Young* [1993], and *Twomey* [1959] Model CDNC Predictions[a]

	CDNC, cm^{-3}		
	UWyo Model	*Young* [1993]	Twomey Model
	Maritime CCN[b]		
Condensation coefficient			
0.01	172	NA	103
0.03	140	155	103
0.09	114	NA	103
0.27	103	NA	103
0.81	103	NA	103
	Continental CCN[c]		
Condensation coefficient			
0.01	639	NA	417
0.03	510	602	417
0.09	439	NA	417
0.27	407	NA	417
0.81	407	NA	417

[a]The UWyo and *Young* [1993] models were initialized at T = 10°C, P = 900 hPa, RH = 95%. These conditions correspond to a cloud base at T = 9.1°C, P = 890 hPa. The form the *Twomey* [1959] model utilized is from *Johnson* [1981]. A vertical speed of 2 m/s was used for all simulations. For the UWyo and models the CCN is pure ammonium sulfate, dry particle masses range from 10^{-22} to 10^{-14} kg, and the thermal accommodation coefficient is unity. For the UWyo and Twomey models droplet concentrations are evaluated at 69 m above cloud base. The Twomey parameter (C) is assumed at T = 25°C and P = 900 hPa. NA = not available.
[b]C = 100 cm^{-3}; k = 0.7.
[c]C = 600 cm^{-3}; k = 0.5.

Notation

a	*Tang* [1996] or *Tang and Munkelwitz* [1994] fitting coefficients
a_w	water activity
c	*Tang* [1996] or *Tang and Munkelwitz* [1994] fitting coefficients
c_p	isobaric specific heat capacity
C	number of droplets or CCN concentration at 1% supersaturation
[*CCN*]	CCN concentration
D_d	dry diameter
D_{se}	sphere equivalent diameter
D_{me}	mobility equivalent diameter
g	acceleration due to gravity
i	van't Hoff factor
k	power law slope of CCN activation spectrum
l	latent heat
m	solute molality
M	molecular weight
n	particle concentration
N	number of particles or concentration of CCN
r	water substance (vapor or liquid) mixing ratio
R	universal gas constant
S	supersaturation
$\hat{S}$	saturation ratio
T	temperature
v	parcel volume corresponding to a unit mass of dry air
u	airspeed
w	vertical velocity
x	salt weight fraction in the solution
z	sampling section
ε	water-soluble mass fraction
Δt	sample duration or time step
ΔT	temperature increment
Δr	mixing ratio increment
σ	surface tension
ρ	density
Ω	rate of increase of surface tension with solute molality
Ψ	coefficient in droplet growth equation
τ	characteristic time for droplet growth

[76] **Acknowledgments.** The authors acknowledge insightful discussions with Erik Swietlicki, Markus Petters and Peter Liu. The APS and growth factor data sets were obtained from archives maintained by the Joint Research Centre of the European Commission and were analyzed with the help of Erik Swietlicki. This work was supported by National Science Foundation grants ATM-9816119 and ATM-0103951, and by the European Union grant EVK2-CT-1999-00054.

References

Abdul-Razzak, H., and S. Ghan, A parameterization of aerosol activation: 2. Multiple aerosol types, *J. Geophys. Res.*, *105*, 6837–6844, 2000.
Bigg, E. K., Discrepancy between observation and prediction of concentrations of cloud condensation nuclei, *Atmos. Res.*, *20*, 82–86, 1986.
Boers, R., P. B. Krummel, S. T. Siems, and G. D. Hess, Thermodynamic structure and entrainment of stratocumulus over the southern ocean, *J. Geophys. Res.*, *103*, 16,637–16,650, 1998.
Brenguier, J. L., T. Bourrianne, A. A. Coelho, J. Isbert, R. Peytavi, D. Trevarin, and P. Wechsler, Improvements of the droplet size distribu-

tion measurements with the Fast-FSSP, *J. Atmos. Oceanic Technol.*, *15*, 1077–1090, 1998.
Brown, E. N., Measurement uncertainties of the NCAR air motion system, *NCAR Tech. Note, NCAR/TN-386+STR*, 1993.
Burnet, F., and J.-L. Brenguier, Comparison between standard and modified forward scattering spectrometer probes during the Small Cumulus Microphysics Study, *J. Atmos. Oceanic Technol.*, *19*, 1516–1531, 2002.
Cantrell, W. G. Shaw, G. R. Cass, Z. Chowdhury, L. S. Hughes, K. A. Prather, S. A. Guazzotti, and K. R. Coffee, Closure between aerosol particles and cloud condensation nuclei at Kaashidhoo Climate Observatory, *J. Geophys. Res.*, *106*, 28,711–28,718, 2001.
Chuang, P. Y., R. J. Charlson, and J. H. Seinfeld, Kinetic limitations on droplet formation in clouds, *Nature*, *390*, 594–596, 1997.
Chuang, P. Y., D. R. Collins, H. Pawlowska, J. R. Snider, H. H. Jonsson, J. L. Brenguier, R. C. Flagan, and J. H. Seinfeld, CCN measurements during ACE-2 and their relationship to cloud microphysical properties, *Tellus, Ser. B*, *52*, 842–866, 2000.
Chýlek, P., and J. G. D. Wong, Erroneous use of the modified Köhler equation in cloud and aerosol physics applications, *J. Atmos. Sci.*, *55*, 1473–1477, 1998.
Covert, D. S., J. L. Gras, A. Wiedensohler, and F. Stratmann, Comparison of directly measured CCN with CCN modeled from the number-size distribution in the marine boundary layer during ACE 1 at Cape Grim, Tasmania, *J. Geophys. Res.*, *103*, 16,597–16,608, 1998.
Delene, D., and T. Deshler, Calibration of a photometric cloud condensation nucleus counter designed for deployment on a balloon package, *J. Atmos. Oceanic Technol.*, *17*, 459–467, 2000.
Delene, D., T. Deshler, P. Wechsler, and G. Vali, A balloon-borne cloud condensation nuclei counter, *J. Geophys. Res.*, *103*, 8927–8934, 1998.
Feingold, G., and P. Y. Chuang, Analysis of the influence of film-forming compounds on droplet growth: Implications for cloud microphysical processes and climate, *J. Atmos. Sci.*, *59*, 2006–2018, 2002.
Fitzgerald, J. W., Dependence of the supersaturation spectrum of CCN on aerosol size distribution and composition, *J. Atmos. Sci.*, *30*, 628–634, 1973.
Fitzgerald, J. W., Effect of aerosol composition on cloud droplet size distribution: A numerical study, *J. Atmos. Sci.*, *31*, 1358–1367, 1974.
Fitzgerald, J. W., Approximate formulas for the equilibrium size of an aerosol particle as a function of its dry particle size and composition and the ambient relative humidity, *J. Appl. Meteorol.*, *14*, 1044–1049, 1975.
Fitzgerald, J. W., and P. Spyers-Duran, Changes in cloud nucleus concentration and cloud droplet size distribution associated with pollution from St. Louis, *J. Appl. Meteorol.*, *30*, 511–516, 1973.
Ghan, S. J., C. Chuang, and J. E. Penner, A parameterization of cloud droplet nucleation, part I: Single aerosol type, *Atmos. Res.*, *30*, 197–222, 1993.
Gerber, H. E., W. A. Hoppel, and T. A. Wojciechowski, Experimental verification of the theoretical relationship between size and critical supersaturation of salt nuclei, *J. Atmos. Sci.*, *34*, 1836–1841, 1977.
Gras, J. L., CN, CCN and particle size in southern ocean air at Cape Grim, *Atmos. Res.*, *35*, 233–251, 1995.
Guibert, S., Validation experimentale des parameterisations de l'effet indirect des aerosols, doctoral dissertation, Univ. e Toulouse III-Paul Sabatier, France, 2002.
Guibert, S., J. R. Snider, and J.-L. Brenguier, Aerosol activation in marine stratocumulus clouds: 1. Measurement validation for a closure study, *J. Geophys. Res.*, *108*(D15), 8628, doi:10.1029/2002JD002678, in press, 2003.
Hallberg, A., et al., Microphysics of clouds: Model versus measurements, *Atmos. Environ.*, *31*, 2453–2462, 1997.
Hallberg, A., K. J. Noone, and J. A. Ogren, Aerosol particles and clouds: Which particles form cloud droplets?, *Tellus, Ser. B*, *50*, 59–75, 1998.
Hämeri, K., A. Laaksonen, M. Väkavä, and T. Suni, Hygroscopic growth of ultrafine sodium chloride particles, *J. Geophys. Res.*, *106*, 20,749–20,757, 2001.
Hinds, W. C., *Aerosol Technology*, John Wiley, Hoboken, N. J., 1999.
Hoppel, W. A., Measurement of the size distribution and CCN supersaturation spectrum of submicron aerosols over the ocean, *J. Atmos. Sci.*, *36*, 2006–2015, 1979.
Ji, Q., and G. E. Shaw, On supersaturation spectrum and size distributions of cloud condensation nuclei, *Geophys. Res. Lett.*, *25*, 1903–1906, 1998.
Johnson, D. B., Analytical solutions for cloud-drop concentration, *J. Atmos. Sci.*, *38*, 215–218, 1981.
Katz, J. L., and P. Mirabel, Calculation of supersaturation profiles in thermal diffusion cloud chambers, *J. Atmos. Sci.*, *32*, 646–652, 1975.
Kelly, W. P., and P. H. McMurry, Measurement of particle density by inertial classification of differential mobility-generated monodisperse aerosols, *Aerosol Sci. Technol.*, *17*, 199–212, 1992.
Knutson, E. O., and K. T. Whitby, Aerosol classification by electric mobility: Apparatus, theory and applications, *J. Aerosol Sci.*, *6*, 443–451, 1975.
List, R. J., *Smithsonian Meteorological Tables*, Smithsonian Inst., Washington, D. C., 1984.
Martinsson, B. G., et al., Validation of very high cloud droplet number concentrations in air masses transported during thousands of kilometers over the ocean, *Tellus, Ser. B*, *52*, 801–814, 2000.
Novakov, T., T. S. Bates, and P. K. Quinn, Shipboard measurements of concentrations and properties of carbonaceous aerosols during ACE-2, *Tellus, Ser. B*, *52*, 228–238, 2000.
Pawlowska, H., and J.-L. Brenguier, Microphysical properties of stratocumulus clouds during ACE-2, *Tellus, Ser. B*, *52*, 868–887, 2000.
Pruppacher, H. R., and J. D. Klett, *Microphysics of Clouds and Precipitation*, Kluwer Acad., Norwell, Mass., 1997.
Putaud, J.-P., R. Van Dingenen, M. Mangoni, A. Virkkula, and F. Raes, Chemical mass closure and origin assessment of the submicron aerosol in the marine boundary layer and the free troposphere at Tenerife during ACE-2, *Tellus, Ser. B*, *52*, 141–168, 2000.
Quinn, P. K., D. S. Covert, T. S. Bates, V. N. Kapustin, D.C. Ramsey-Bell, and L. M. McInnes, Dimethylsulfide/cloud condensation nuclei/climate system: Relevant size-resolved measurements of the chemical and physical properties of atmospheric aerosol particles, *J. Geophys. Res.*, *98*, 10,411–10,427, 1993.
Quinn, P. K., T. S. Bates, D. J. Coffman, T. L. Miller, J. E. Johnson, D. S. Covert, J.-P. Putaud, C. Neusüß, and T. Novakov, A comparison of aerosol chemical and optical properties from the 1st and 2nd Aerosol Characterization Experiments, *Tellus, Ser. B*, *52*, 239–257, 2000.
Seinfeld, J. H., and S. N. Pandis, *Atmospheric Chemistry and Physics*, John Wiley, Hoboken, N. J., 1998.
Shaw, R. A., and D. Lamb, Experimental determination of the thermal and condensation coefficients of water, *J. Chem. Phys.*, *111*, 10,659–10,663, 1999.
Shulman, M. L., M. C. Jacobson, R. J. Charlson, R. E. Synovec, and T. E. Young, Dissolution behavior and surface tension effects of organic compounds in nucleating cloud droplets, *Geophys. Res. Lett.*, *23*, 277–280, 1996.
Sioutas, C., E. Abt, J. M. Wolfson, and P. Koutrakis, Evaluation of the measurement performance of the scanning mobility particle sizer and aerodynamic particle sizer, *Aerosol Sci. Technol.*, *30*, 84–92, 1999.
Snider, J. R., and J.-L. Brenguier, A comparison of cloud condensation nuclei and cloud droplet measurements obtained during ACE-2, *Tellus, Ser. B*, *52*, 828–842, 2000.
Squires, P., Diffusion chambers for the measurement of the spectrum of critical supersaturations of cloud nuclei, in *The Second International Workshop on Condensation and Ice Nuclei*, edited by L. O. Grant, pp. 7–10, Dept. of Atmos. Sci., Colorado State Univ., Fort Collins, 1971.
Swietlicki, E., et al., Hygroscopic properties of aerosol particles in the north-eastern Atlantic during ACE-2, *Tellus, Ser. B*, *52*, 201–227, 2000.
Tang, I. N., Chemical and size effects of hygroscopic aerosols on light scattering coefficients, *J. Geophys. Res.*, *101*, 19,245–19,250, 1996.
Tang, I. N., and H. R. Munkelwitz, Water activities, densities, and refractive indices of aqueous sulfates and sodium nitrate droplets of atmospheric importance, *J. Geophys. Res.*, *99*, 18,801–18,808, 1994.
Twomey, S., The nuclei of natural cloud formation. Part II: The supersaturation in natural clouds and the variation of cloud droplet concentration, *Geofis. Pura Appl.*, *43*, 243–249, 1959.
Twomey, S., and J. Warner, Comparison of measurements of cloud droplets and cloud nuclei, *J. Atmos. Sci.*, *24*, 702–703, 1967.
Van Dingenen, R., F. Raes, J.-P. Putaud, A. Virkkula, and M. Mangoni, Processes determining the relationship between aerosol number and non-sea-salt sulfate mass concentrations in the clean and perturbed marine boundary layer, *J. Geophys. Res.*, *104*, 8027–8038, 1999.
VanZanten, M. C., P. G. Duynkerke, and J. W. M. Cuijpers, Entrainment parameterization in convective boundary layers derived from large eddy simulations, *J. Atmos. Sci.*, *56*, 813–828, 1999.
Weiss, D. D., and G. E. Ewing, Water content and morphology of sodium chloride aerosol particles, *J. Geophys. Res.*, *104*, 21,275–21,285, 1999.
Wood, R., et al., Boundary layer and aerosol evolution during the third Lagrangian experiment of ACE-2, *Tellus, Ser. B*, *52*, 401–422, 2000.

Young, K., Effects of simplifications of the Köhler equation on the activation of CCN in an updraft, *J. Atmos. Sci.*, *50*, 2314–2317, 1993.

Young, K., and A. J. Warren, A reexamination of the derivation of the equilibrium supersaturation curve for soluble particles, *J. Atmos. Sci.*, *49*, 1138–1143, 1992.

Yum, S. S., J. G. Hudson, and Y. Xie, Comparisons of cloud microphysics with cloud condensation nuclei spectra over the summertime Southern Ocean, *J. Geophys. Res.*, *103*, 16,625–16,636, 1998.

Zhou, J., E. Swietlicki, O. H. Berg, P. P. Aalto, K. Hämeri, E. D. Nilsson, and C. Leck, Hygroscopic properties of aerosol particles over the central Arctic Ocean during summer, *J. Geophys. Res.*, *106*, 32,111–32,123, 2001.

Zou, Y.-S., and N. Fukuta, The effect of diffusion kinetics on the supersaturation in clouds, *Atmos. Res.*, *52*, 115–141, 1999.

J.-L. Brenguier and S. Guibert, Centre National de Recherche Météorologique (CNRM), GMEI/D, Météo-France, 42 Avenue Coriolis, F-31057 Toulouse Cedex 01, France. (jlb@meteo.fr; guibert@cnrm.meteo.fr)

J.-P. Putaud, European Commission, Joint Research Centre, Institute for Environment and Sustainability, via Fermi, 1, Ispra, I-21020, Italy. (jean.putaud@jrc.it)

J. R. Snider, Department of Atmospheric Science, University of Wyoming, Laramie, WY 82701, USA. (jsnider@uwyo.edu)